**Tutorial**

# Synthesis of Parametrically Coupled Networks

Ofer Naaman [1,*] and José Aumentado [2,†]

[1] *Google Quantum AI, Santa Barbara, California 93117, USA*
[2] *National Institute of Standards and Technology, Boulder, Colorado 80305, USA*

We show that a common language can be used to unify the description of parametrically coupled circuits—parametric amplifiers, frequency converters, and parametric nonreciprocal devices—with that of band-pass filter and impedance matching networks. This enables one to readily adapt network synthesis methods from microwave engineering in the design of parametrically coupled devices having prescribed transfer characteristics, e.g., gain, bandwidth, return loss, and isolation. We review basic practical aspects of coupled-mode theory and filter synthesis, and then show how to apply both, on an equal footing, to the design of multipole, broadband parametric and nonreciprocal networks. We supplement the discussion with a range of examples and reference designs.

**CONTENTS**

---

*ofernaaman@google.com
†jose.aumentado@boulder.nist.gov

# I. INTRODUCTION

The success of Josephson parametric amplifiers in enabling high-fidelity readout of superconducting qubits has led to a flurry of research into parametrically coupled networks, including amplifiers, frequency converters, and parametric nonreciprocal networks [1–3]. While much of the recent parametric amplifier activity is aimed at increasing amplifier saturation power and bandwidth [4–8], a parallel research path has focused on generating nonreciprocal frequency conversion and amplification—an effort motivated by the need to improve qubit isolation from noise in the measurement chain, with the ultimate goal of minimizing the reliance on bulky ferrite circulators [9–14]. Recent work on parametric conversion has additionally expanded into electro-optomechanical systems [15–17], specifically facilitating the use of mechanical modes to mediate electrical to optical transduction.

Despite significant progress, we make the following observations: (a) there is currently no methodology in place to engineer the transfer characteristics (e.g., bandwidth, ripple, gain, return loss, etc.) of parametrically coupled devices to arbitrary (physically realisable) specifications, and (b) there is no unified language for including parametrically coupled devices on an equal footing with the electrical, mechanical, optical, or hybrid circuit in which they may be embedded.

In this tutorial, we show that the problem of designing parametrically coupled circuits can be mapped onto a band-pass network synthesis problem. In doing so, we establish a common language to describe parametric interactions as circuit elements—this allows one to design and simulate general circuits that involve both parametric and passive coupling between multiple resonant modes, while also bringing band-pass network synthesis methods to bear on the design of more complicated parametrically coupled devices. To be clear, this approach is applicable to any system that can be described by a system of linear coupled-mode equations, including both resonant and parametric coupling on equal footing.

This tutorial is organized as follows. In Sec. II we briefly summarize the coupling-graph approach and associated coupling-matrix formalism described in Refs. [9,18, 19], which provide a convenient way to visualize parametrically coupled circuits and calculate their $S$ parameters. In Sec. III we discuss parametric couplers and show that they function as generalized admittance or impedance inverters—common in microwave-engineering circuit design as critical elements in the design of filter and impedance matching networks. Next, we briefly outline in Sec. IV some basic concepts and methods in band-pass network synthesis, and in Sec. V we unify the microwave-engineering language of band-pass network synthesis with that of conventional coupled-mode theory. We apply the concepts developed throughout the preceding sections to design a range of parametrically coupled devices: a broadband parametric converter, a broadband parametric circulator, and a broadband nondegenerate Josephson parametric amplifier, all combining both passive (resonant) and parametric couplings to achieve a specific target response.

## II. COUPLING MATRICES AND GRAPHS

### A. Coupling matrix formalism

In this section we sketch a formalism for the analysis and visualization of coupled-mode networks, define terminology, and establish notational conventions. The formalism that we use is based on Ref. [18], which was later employed in Refs. [9,12,19,20]. We show how to describe an arbitrary network of resonantly or parametrically coupled modes by a coupled-mode equation of motion matrix **M**, and how the input-output boundary condition [21] can be used to derive a generalized multiport scattering matrix ($S$ parameters). Although this approach was developed in the context of parametrically coupled networks, it is equally adept at describing networks with constant (passive) coupling, providing a flexible description that can be used to combine physical matching networks with parametric frequency conversion and amplification.

We consider a set of resonant modes having natural frequencies $\{\omega_k\}$. Each mode is characterized by a complex mode amplitude $a_k$, such that $a_k^* a_k = n_k$ is the number of photons in mode $k$. For example, in an electrical circuit we

may define [22]

$$a_k = \frac{1}{\sqrt{2\hbar Z_k}}L_k I_k + i\sqrt{\frac{Z_k}{2\hbar}}C_k V_k, \qquad (1)$$

where $L_k$ ($C_k$) is the inductance (capacitance) of the mode, $Z_k = \sqrt{L_k/C_k}$ is the mode impedance, $I_k$ is the mode current, and $V_k$ is the mode voltage. Note that here $a_k$ is the classical mode amplitude and the choice to scale to the square root photon (or phonon) number is a convenient correspondence to its formal annihilation operator counterpart. We note that the coupling description given here yields the same linear scattering matrix one would derive with a more rigorous quantum approach (cf. Ref. [19]).

The equations of motion of an arbitrary linear coupled-mode system can then be cast in terms of these complex amplitudes $a_j(t)$,

$$\dot{a}_j = -i\left(\omega_j - i\frac{\gamma_j}{2}\right)a_j - i\sum_{k\neq j} c_{jk}(a_k + a_k^*) + \sqrt{\gamma_j^{\text{ext}}}a_j^{\text{in}}, \qquad (2)$$

where we have included the drive term $a_j^{\text{in}}$, and $j$ spans the set of resonances or resonators. The dissipation rate $\gamma_j = \gamma_j^{\text{int}} + \gamma_j^{\text{ext}}$ is the sum of the mode's internal dissipation, $\gamma_j^{\text{int}}$, and external loading, $\gamma_j^{\text{ext}}$, due to coupling out through the signal ports. In an electrical circuit, the dissipation rate is simply $\gamma = 1/RC$, where $R$ is the equivalent shunt resistance seen by a parallel resonant circuit (in recent literature, this quantity is often denoted as $\kappa$, but we choose to maintain here the notation of Ref. [18]). The drive term corresponds to incident propagating waves with a rate $|a_j^{\text{in}}|^2$ quanta (e.g., photons or phonons) per second. The coefficients $c_{jk}$ are coupling rates (often denoted as $g$, but we reserve this symbol to later signify filter prototype coefficients), and can be constant, modulated (time varying), or some combination of the two. For instance, in an all passive electrical network these couplings might be realized by mutual inductances or coupling capacitors between resonators, while in a parametric amplifier or frequency converter, these elements can be varactors (tunable capacitors) [23] or Josephson junctions [1].

### 1. The equation-of-motion matrix M

To determine the driven response of this coupled system, it is more convenient to Fourier transform the equations of motion, Eq. (2). In a parametrically coupled multimode system, one finds solutions that correspond to oscillations in each resonator, often at several different frequencies because of mixing terms generated by coupling modulation. If we relabel the Fourier frequency variable $\omega \rightarrow \omega_j^s$ to correspond to one of the input drives into the $j$th resonator at frequency $\omega_j^s$ (the superscript $s$ is for *signal* or

*stimulus*), the system can respond both at $\omega_j^s$ as well as mixing products generated by the coupling modulation. The family of resonator response amplitudes, at all possible mixing product frequencies, comprises the set of possible steady-state solutions to the driven equations of motion, Eq. (2). We can write the *internal* mode amplitudes in the Fourier domain as the set $\vec{v} = \{a_j[\omega_j^s]\}$. In general, one may annotate the mode amplitudes according to the resonator wherein they reside, and an additional label to indicate a specific mixing product within that resonance; we suppress these additional bookkeeping details here for clarity. The vector $\vec{v}$ can additionally include conjugate mode amplitudes. For each of the amplitudes in $\vec{v}$, we can assign a corresponding drive, and the set of all drive terms can be represented by $\vec{v}_{\text{in}} = \{a_j^{\text{in}}[\omega_j^s]\}$. In this basis we can write Eq. (2) in a compact matrix form,

$$-i\gamma_0 \mathbf{M}\vec{v} = \mathbf{K}\vec{v}_{\text{in}}. \qquad (3)$$

The matrix $\mathbf{M}$ encapsulates the frequency-domain equations of motion, describing how energy is coupled between oscillating fields and their mixing products. The matrix $\mathbf{K}$ describes external dissipation for all modes in the mode basis, $\mathbf{K} \equiv \text{diag}(\{\sqrt{\gamma_j^{\text{ext}}}\})$. The prefactor $\gamma_0$ is an overall normalization—a characteristic rate in the system—whose form is chosen to suit different physical problems, as we discuss below.

It is important to note that, in general, the complete mode basis can be quite large, yet many of these mode amplitudes are far off resonant, and do not contribute to the steady-state dynamics. It is therefore customary to reduce the mode basis $\vec{v}$ by performing rotating wave approximations, eliminating modes whose frequencies are fast with respect to their corresponding host resonance natural frequency, i.e., if $|\omega_j^s - \omega_j| \gg \gamma_j$.

The structure of $\mathbf{M}$ has a very simple general form,

$$\mathbf{M} = \begin{bmatrix} \Delta_1 & \beta_{12} & \cdots & \beta_{1N} & \beta_{11*} & \cdots & \beta_{1N*} \\ \beta_{21} & \Delta_2 & \cdots & \beta_{2N} & \beta_{21*} & \cdots & \beta_{2N*} \\ \vdots & & \ddots & \vdots & \vdots & \ddots & \vdots \\ \beta_{N1} & \cdots & & \Delta_N & \beta_{N1*} & \cdots & \beta_{NN*} \\ \beta_{1*1} & \cdots & & \beta_{1*N} & -\Delta_1^* & \cdots & \beta_{1*N*} \\ \vdots & & & \vdots & \vdots & \ddots & \vdots \\ \beta_{N*1} & \cdots & & \beta_{N*N} & \beta_{N*1*} & \cdots & -\Delta_N^* \end{bmatrix}, \qquad (4)$$

where we define the diagonal detuning terms

$$\Delta_k \equiv \frac{1}{\gamma_0}\left(\omega_k^s - \omega_k + i\frac{\gamma_k}{2}\right) \qquad (5)$$

and the off-diagonal coupling terms

$$\beta_{jk} = \frac{c_{jk}}{2\gamma_0}. \tag{6}$$

The normalized coupling rates $|\beta_{jk}|^2$ are related to the cooperativity parameter in cavity QED [24], circuit QED [25], or optomechanics [26].

There are four main blocks in $\mathbf{M}$ in Eq. (4): the block-diagonal represents passive or frequency-conversion (difference-frequency) coupling within the mode manifold (upper left $N \times N$ block) and anti-conjugate-mode manifold (lower right block); the off-diagonal $N \times N$ blocks represent parametric amplification coupling (sum frequency) between the two manifolds. Often, the connectivity of the network will result in a total matrix $\mathbf{M}$ that can be reduced to separate redundant matrices with no coupling between them—we henceforth work with the minimal nonredundant subset of modes and submatrix that describes the coupled network of interest. As a concrete minimal example, one could describe the driven response of a single resonator with a two-mode basis, $\vec{v} = (a[\omega_A^s], a^*[-\omega_A^s])^T$, and a $2 \times 2$ $\mathbf{M}$ matrix. In the absence of parametric pumping, the two modes are uncoupled ($\beta_{AA^*} = \beta_{A^*A} = 0$) and it is sufficient to describe the system with a single equation of motion, $-i\gamma_A \Delta_A a[\omega_A^s] = \sqrt{\gamma_A^{\text{ext}}} a^{\text{in}}[\omega_A^s]$, since the other equation of motion is just the conjugate of this equation. If, on the other hand, the resonator is parametrically pumped with $\omega_P \simeq 2\omega_A$, the modes $a[\omega_A^s]$ and $a[\omega_A^s - \omega_P]$ are coupled and the full $2 \times 2$ $\mathbf{M}$ matrix is required. We refer the reader to Ref. [18] for a more detailed treatment.

The coupling coefficients $\beta_{jk}$ follow a particular pattern that is determined by the coupling mechanism [18]. If the coupling is passive, they are symmetric and real, $\beta_{jk} = \beta_{kj} \in \mathbb{R}$. If the coupling corresponds to frequency conversion, that is, the physical coupling element is modulated at the difference frequency between modes $j$ and $k$, the coupling coefficients are related by conjugation, $\beta_{jk} = \beta_{kj}^*$. Lastly, if the coupling is modulated at the sum frequency, generating amplification, the coefficients are related by anticonjugation, $\beta_{jk} = -\beta_{kj}^*$.

The simple structure of $\mathbf{M}$ allows one, with experience, to identify the relevant mode basis quickly, and assign the appropriate conjugation and signs to the coupling, building a picture of the dynamics within a system.

### 2. Generalized scattering

The input and output drive amplitudes, $\vec{v}_{\text{in}}$ and $\vec{v}_{\text{out}}$, obey a boundary condition at each port, which connects them to the internal mode amplitudes [21,27], $\vec{v}_{\text{in}} + \vec{v}_{\text{out}} = \mathbf{K}\vec{v}$. From this, together with Eq. (3), one can compute the full scattering matrix

$$\mathbf{S} = i\frac{1}{\gamma_0}\mathbf{K}\mathbf{M}^{-1}\mathbf{K} - \mathbb{I}. \tag{7}$$

It is useful to write this in component form:

$$S_{jk} = \frac{a_j^{\text{out}}}{a_k^{\text{in}}} = i\frac{\sqrt{\gamma_j^{\text{ext}}\gamma_k^{\text{ext}}}}{\gamma_0}\left[\mathbf{M}^{-1}\right]_{jk} - \delta_{jk}. \tag{8}$$

When all coupling in the network is passive, there is no frequency translation and Eq. (8) describes scattering between physical input and output ports. It is then essentially identical to its electrical engineering counterpart—the usual $S$ parameters of the network. However, the presence of time-varying, modulated coupling generates scattering between frequencies, both within single resonators as well as between different physical resonators and Eq. (8) is broadly defined to include scattering between mode amplitudes rotating at different frequencies. One other notable difference between our definition above and the usual $S$ parameters is that here, scattering is defined as the ratio of output to input mode amplitudes that we have chosen to normalize to energy quanta, $\hbar\omega_k^s$; see Eq. (1). By contrast, scattering parameters in electrical engineering are commonly defined by the ratio of the equivalent voltage amplitudes, $S_{jk} \equiv V_j^{\text{out}}/V_k^{\text{in}}$ [28]. A consequence of this difference in definition is that a process having unity gain in our convention will be associated with a gain factor in the common electrical engineering definition of the scattering parameters, stemming from the Manley-Rowe relations [29]. An example of this difference is discussed in Sec. V B.

### 3. Simplifications for network synthesis

In the above, we have cast the problem of mode coupling in a linear system as generally as possible, following the prescription in Ref. [18]. However, for the purpose of the present discussion, we can perform some simplifications to this model to focus on the specific problem of network synthesis and amplifier or converter design. Namely, we assume that only a subset of the modes are coupled to signal ports, and further consider the ideal case where there is no internal loss.

As an example, a simple two-port microwave $N$-pole cavity filter will have $N$ cavities, each with extremely low internal loss, but since it is connected to input and output ports at the ends, $\gamma_1$ and $\gamma_N$ present the only available dissipation channels. In other words, the total dissipation rates of the "internal" modes can be set to zero, $\{\gamma_2, \ldots, \gamma_{N-1}\} = 0$, and the subset of scattering elements,

$$\mathbf{S} = \begin{bmatrix} S_{11} & S_{1N} \\ S_{N1} & S_{NN} \end{bmatrix}, \tag{9}$$

is sufficient to describe the filter response. To this end, we mark a subset of the modes as *ports*, $\mathcal{P} \subset \{v_j\}$, through which energy can be injected and extracted, and set all mode dissipations and input drives to zero, $\gamma_k = 0$, $v_k^{\text{in}} = 0$, for everything that is not a port. Likewise, since the total dissipation of a resonator $k$ is the sum of its internal and external losses, $\gamma_k = \gamma_k^{\text{int}} + \gamma_k^{\text{ext}}$, the "no internal loss" assumption means that $\gamma_k = \gamma_k^{\text{ext}}$ and we can drop the "int" and "ext" superscripts in the remainder of this tutorial. In this same spirit, we choose a form for the normalization rate that is the geometric mean of the dissipations of all connected ports,

$$\gamma_0 \equiv \sqrt[N_{\mathcal{P}}]{\prod_{k \in \mathcal{P}} \gamma_k}, \tag{10}$$

where $N_{\mathcal{P}}$ is the number of ports. For the two-port example above, $\gamma_0 = \sqrt{\gamma_1 \gamma_N}$. Modes that are marked as ports can additionally be characterized with a finite quality factor

$$Q_j = \frac{\omega_j}{\gamma_j}. \tag{11}$$

Since in the rest of this tutorial we focus on the problem of network synthesis primarily through the lens of electrical circuit design, it will be convenient to connect the notion of input admittance to the general picture presented thus far. These are connected by inverting the usual formula for the reflection coefficient in terms of input admittance, $Y_{\text{in}} = Y_0(1 - S_{kk})/(1 + S_{kk})$. One can then show that the admittance, looking into resonator $k$ at mode frequency $\omega_k^s$, is

$$Y_{\text{in}} = -Y_0 \left[ 2i \frac{\gamma_0}{\gamma_k} \frac{1}{[\mathbf{M}^{-1}]_{kk}} + 1 \right], \tag{12}$$

where $Y_0$ is the reference admittance of the environment connected to port $k$, usually taken to be $(50\ \Omega)^{-1}$.

### 4. Internal dissipative losses

We proceed for the remainder of this tutorial with the "zero internal loss" assumption. This assumption is reasonable for implementations based on superconducting circuits and microwave cavities; however, in optomechanical circuits internal losses play a more central role [26]. Furthermore, any accurate analysis of quantum noise in parametric networks must include all internal dissipation sources.

The topic of coupled-resonator network design techniques in the presence of internal dissipative losses has received considerable attention in the microwave engineering literature, and we point the reader to, e.g., Refs. [30–32]. As we will see throughout this tutorial, network synthesis techniques from microwave engineering can be readily adopted in parametrically coupled circuits.

Noise properties of coupled-mode systems can be calculated using the equation-of-motion matrix formalism described in this section by including all internal losses as effective ports [19,33]. The simplifications made in Sec. II A 3 are useful in network synthesis, and the resulting ideal networks can then be reannotated to include finite temperature dissipation sources for the purpose of noise calculations. This general noise analysis approach is beyond the scope of this tutorial.

### B. Coupled-mode graph representation

The formalism described in Sec. II A provides a method for calculating $S$ parameters for driven modes within an arbitrary system of coupled resonators, where ports are generalized to both physical and frequency space and the couplings can be complex, carrying the phases of the pumps driving them. This allows one to include both parametric coupling processes (amplification and frequency conversion) and passive coupling structures in a straightforward way, but requires careful bookkeeping. In multiple-resonator systems, the addition of even a few parametric couplings can generate a surprising increase in the mode basis size (see, e.g., Refs. [13,20,34]). While this accounting can, with care, be automated in a numerical calculation, one can also utilize a graph representation [9,18,19] that facilitates bookkeeping and serves as an aid in analysis, design, and synthesis.

Since the coupled-mode equation-of-motion matrix $\mathbf{M}$ is square, it can be represented as a directed graph [35,36], where each of the modes can be represented as a node. In this picture, we represent the diagonal elements, $\Delta_k$, as self-loops, connecting a node to itself, while all off-diagonal couplings $\beta_{jk}$ are represented by directed edges (arrows) that connect one node to another. Above, we outlined rules for relating $\beta_{jk}$ to $\beta_{kj}$ based on the nature of the coupling. With these rules, one can derive the equations of motion of a linear coupled-mode system quickly, simply by drawing a graph and identifying all of the coupling signs and conjugations correctly by inspection.

Graph primitives for one- and two-mode processes are given in the left-hand column in Fig. 1 along with the rules for writing their corresponding matrix elements. After identifying the graph representation, one can immediately obtain the equation-of-motion matrix $\mathbf{M}$, and from it scattering parameters via Eq. (8). From these primitives, one can construct more complex networks such as multimode parametric amplifiers [9,10,12,18,20] and hybrid optomechanical circuits [13], which rely on the topology of the network to produce directionality and phase-sensitive amplification.

Since there are only three possible mechanisms for coupling—resonance (passive coupling), parametric frequency conversion (modulated at the difference frequency), and parametric amplification (modulated at the

FIG. 1.   Rules for writing the equation-of-motion matrix elements of a system from its graph representation. Left column: graph primitives using the notation of Ref. [18]; second column: corresponding coupling process; third column: matrix elements and their conjugation relations; right column: abbreviated notation used in this tutorial.

sum frequency)—with well-defined relationships between forward and backward couplings, we can simplify the graph representation to show all directed edge pairs ($\beta_{jk}$ and $\beta_{kj}$) as single (resonant) or double lines (parametric). Parametric frequency conversion and amplification are further distinguished by whether they connect corotating or counter-rotating (conjugated) modes, indicated by mode labels and face color for each node. Figure 1 summarizes the translation between the original directed graph notation of Ref. [18] and the abbreviated notation used in this tutorial, along with the corresponding matrix coupling element conjugation rules.

In the simplified graph representation, we only draw self-loops for modes that are connected to ports and therefore have nonvanishing dissipation.

### C. Examples

Practical use of the tools outlined above is best illustrated through simple canonical examples of parametrically coupled networks. In the examples below, we highlight a design flow that uses the network graph to extract its equation-of-motion matrix, calculate its $S$ parameters, and derive design parameters based on performance requirements.

#### *1. Parametric frequency converter*

The two-mode parametric frequency converter is the simplest nontrivial parametric device. As a concrete

example, one may construct a circuit comprised of two $LC$ resonators, coupled by a modulated mutual inductance [Fig. 2(a)]. The resonators have different natural frequencies, $\omega_A$ and $\omega_B$, and are coupled to external transmission lines with characteristic impedance $Z_0$ through capacitors $C_{cA}$ and $C_{cB}$. Propagating electromagnetic waves ($a^{\text{in/out}}[\omega_A^s]$ and $b^{\text{in/out}}[\omega_B^s]$) can propagate in and out of $A, B$ resonators with rates

$$\gamma_A = \frac{\omega_A^2 C_{cA}^2 Z_0}{C_A}, \tag{13}$$

$$\gamma_B = \frac{\omega_B^2 C_{cB}^2 Z_0}{C_B}. \tag{14}$$

If the natural frequencies differ by more than the bandwidths, $|\omega_A - \omega_B| \gg \sqrt{\gamma_A \gamma_B}$, energy exchange is greatly reduced, but can be recovered if the mutual inductance is pumped (sinusoidally modulated) at the difference frequency, $\omega_P \simeq |\omega_A - \omega_B|$, resulting in frequency conversion—power is transferred from $a^{\text{in}}$ to $b^{\text{out}}$, and from $b^{\text{in}}$ to $a^{\text{out}}$.

The graph representation of the two-mode frequency converter is shown in Fig. 2(b). Using the rules in Fig. 1, we can immediately write the equation-of-motion matrix $\mathbf{M}_{\text{FC}}$ as shown in Fig. 2(b). Here, the equation-of-motion matrix is written in the driven mode basis $\vec{v} = (a[\omega_A^s], b[\omega_B^s])^T$. The detuning terms, including the respective port dissipation rates, are written according to
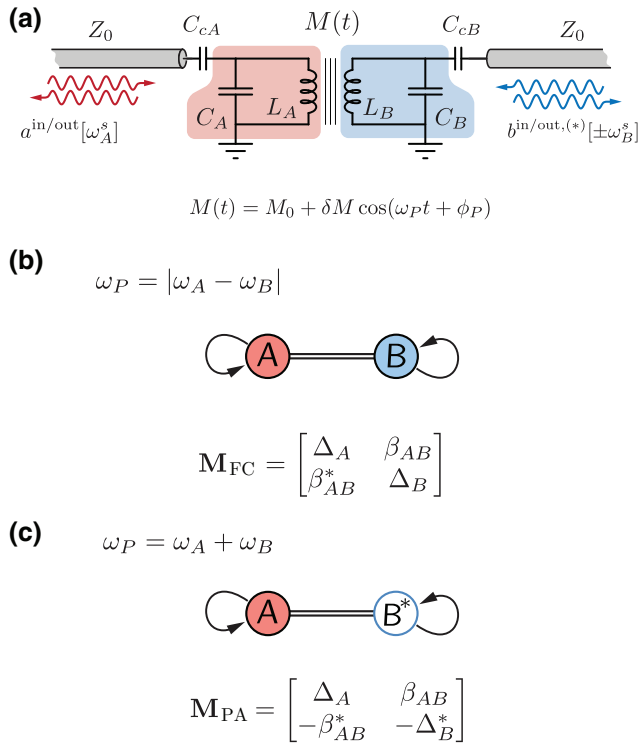
**(a)**



$$M(t) = M_0 + \delta M \cos(\omega_P t + \phi_P)$$

**(b)**

$$\omega_P = |\omega_A - \omega_B|$$



$$\mathbf{M}_{\text{FC}} = \begin{bmatrix} \Delta_A & \beta_{AB} \\ \beta_{AB}^* & \Delta_B \end{bmatrix}$$

**(c)**

$$\omega_P = \omega_A + \omega_B$$



$$\mathbf{M}_{\text{PA}} = \begin{bmatrix} \Delta_A & \beta_{AB} \\ -\beta_{AB}^* & -\Delta_B^* \end{bmatrix}$$

FIG. 2. (a) Schematic of a circuit containing two resonant modes coupled through a time-varying mutual inductance pumped at a frequency $\omega_P$. (b) Coupled-mode graph of a two-mode parametric converter and the corresponding equation-of-motion matrix, written in the basis $\vec{v} = (a[\omega_A^s], b[\omega_B^s])^T$. (c) Coupled-mode graph of a two-mode parametric amplifier and the corresponding equation-of-motion matrix, written in the basis $\vec{v} = (a[\omega_A^s], b^*[-\omega_B^s])^T$.

Eq. (5) as

$$\Delta_A = \frac{1}{\gamma_0}\left( \omega_A^s - \omega_A + i\frac{\gamma_A}{2} \right), \tag{15}$$

$$\Delta_B = \frac{1}{\gamma_0}\left( \omega_A^s + \omega_P - \omega_B + i\frac{\gamma_B}{2} \right), \tag{16}$$

where we have already substituted for $\omega_B^s$ via the pump frequency, $\omega_B^s = \omega_A^s + \omega_P$.

Observe that, since the pump is tuned to the difference frequency, we also have $\omega_P - \omega_B = -\omega_A$, so we could have instead written in Eq. (16) $\Delta_B = (1/\gamma_0)(\omega_A^s - \omega_A + i\gamma_B/2)$. In other words, the fact that the modes are at different frequencies drops out of the equations. We use this insight repeatedly here, keeping in mind that the deviation of the pump frequency from perfect tuning (while beyond the scope of the present discussion) can open additional useful design space in certain applications.

We want to design the network to be impedance matched to the 50 Ω ports. Using Eq. (8), we can write the reflection off of port $A$:

$$S_{AA} = i\frac{\gamma_A}{\gamma_0} \frac{\Delta_B}{\Delta_A \Delta_B - |\beta_{AB}|^2} - 1. \tag{17}$$

At zero detuning, $\omega_A^s - \omega_A = 0$, we have

$$S_{AA} = \frac{1 - 4|\beta_{AB}|^2}{1 + 4|\beta_{AB}|^2}, \tag{18}$$

and requiring $S_{AA} = 0$ for perfect matching results in $|\beta_{AB}| = 0.5$. Furthermore, from the transmission $S_{BA}$ we can calculate $\Delta\omega$, the 3-dB bandwidth of the network, and find that the bandwidth is optimized when $\gamma_A = \gamma_B$, where it is equal to $\Delta\omega = \sqrt{2}\gamma_0$.

Figure 3 shows $S$ parameters in dB versus the signal frequency of a parametric frequency converter designed to meet the following requirements: $\omega_A/2\pi = 5$ GHz, $\omega_B/2\pi = 7$ GHz, and 3-dB bandwidth of $\Delta\omega/2\pi = 100$ MHz. According to the discussion above, we can calculate the port coupling rate $\gamma_0/2\pi = 70.7$ MHz [Eq. (10)], and parametric coupling rate $c_{AB}/2\pi = 2\gamma_0\beta_{AB}/2\pi = 70.7$ MHz [Eq. (6)]. For each signal frequency in Fig. 3, we invert the matrix in Fig. 2(b) and calculate the $S$ parameters using Eq. (8). Note that the inductor and capacitor values are not specified here, and this approach is, instead, cast in terms of frequencies, dissipation, and coupling rates. Specific circuit parameter values can be designed to realize these while accommodating realistic design and fabrication constraints of a chosen technology.

In Sec. V we will see that the converter we designed here exactly implements a two-pole max-flat (Butterworth) response, as Fig. 3 already hints.

In Fig. 3, and all subsequent figures that show $S$ parameters in this tutorial, we use the fact that, when the pump frequency is exactly tuned to the difference (conversion)
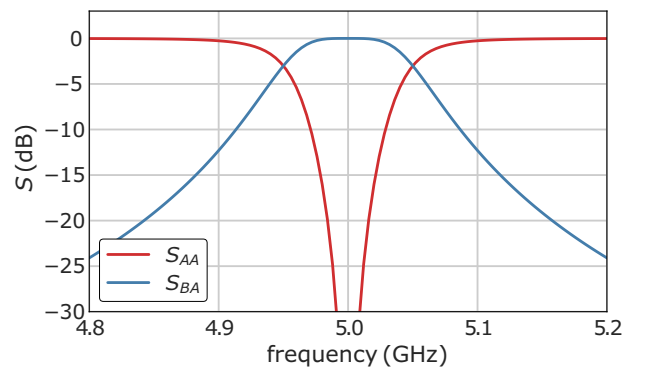


FIG. 3. $S$ parameters of the two-mode frequency converter, calculated using Eq. (8). The frequency axis is referenced to the signal port: $S_{AA}$ is the reflection off of the input port at the indicated frequency, $\omega_A^s/2\pi$; $S_{BA}$ is the conversion gain—output photon flux at port $B$ at $\omega_A^s + \omega_P$ normalized to input flux at port $A$ at frequency $\omega_A^s$.

or sum (amplification) frequency, the problem has a single independent reference frequency variable—indicated on the frequency axis in these figures. Curves that represent $S$ parameters for frequency-translating processes should be understood in relation to that reference frequency where either the input or the output frequency or both correspond to translating the reference frequency by the pump frequency for the corresponding process. Specifically, in Fig. 3, the curve labeled $S_{BA}$ represents the output photon flux at port $B$ at $\omega_A^s + \omega_P$ normalized to input photon flux at port $A$ at frequency $\omega_A^s$, where $\omega_A^s/2\pi$ also serves as the independent frequency variable indicated on the $x$ axis.

### 2. Parametric amplifier

The coupled-mode graph of a two-mode parametric amplifier is shown in Fig. 2(c). The same graph can describe both a degenerate reflection amplifier such as the Josephson Parametric Amplifier (JPA) [37,38] when $\omega_A = \omega_B$ and the same physical resonator hosts both modes, and a nondegenerate amplifier such as the Josephson Parametric Converter (JPC) [39] or Field Programmable Josephson Amplifier (FPJA) [9], where the modes are hosted in physically separate resonators or resonances similar to Fig. 2(a). In this case, the equation-of-motion matrix $\mathbf{M}_{PA}$ is written in the basis $\vec{v} = (a[\omega_A^s], b^*[-\omega_B^s])^T$. Observe that the mode $B$ is now conjugated as indicated by its open face shading and the anticonjugation of the corresponding detuning term $-\Delta_B^*$ in the equation-of-motion matrix. We have again used the rules in Fig. 1 to fill in the off-diagonal elements with the appropriate anticonjugation of $\beta_{BA} = -\beta_{AB}^*$ for a parametric process driven by a sum-frequency pump $\omega_P = \omega_A + \omega_B$. The detuning terms are

$$\Delta_A = \frac{1}{\gamma_0}\left(\omega_A^s - \omega_A + i\frac{\gamma_A}{2}\right), \qquad (19)$$

$$-\Delta_B^* = \frac{1}{\gamma_0}\left(\omega_A^s - \omega_P + \omega_B + i\frac{\gamma_B}{2}\right), \qquad (20)$$

where we have replaced $\omega_B^s = -\omega_A^s + \omega_P$. Since it is also the case that $-\omega_P + \omega_B = -\omega_A$ we could have written instead $-\Delta_B^* = (1/\gamma_0)(\omega_A^s - \omega_A + i\gamma_B/2)$, demonstrating again that, under the resonant pump condition ($\omega_P$ perfectly tuned to the sum frequency), the system has only a single independent frequency variable.

The reflection off of the signal mode $A$ using Eq. (8) is

$$S_{AA} = i\frac{\gamma_A}{\gamma_0}\frac{\Delta_B^*}{\Delta_A\Delta_B^* - |\beta_{AB}|^2} - 1, \qquad (21)$$

and at the center frequency of the amplifier we get

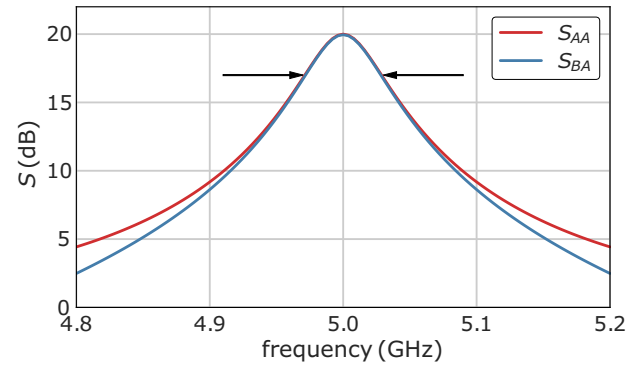$$S_{AA} = \sqrt{G} = \frac{1 + 4|\beta_{AB}|^2}{1 - 4|\beta_{AB}|^2}, \qquad (22)$$



FIG. 4. $S$ parameters of the two-mode parametric amplifier, calculated using the equation-of-motion matrix in Fig. 2(c) and Eq. (8). The frequency axis is referenced to the signal port. Here $S_{AA}$ is the signal reflection gain and $S_{BA}$ is the idler gain. Arrows indicates the 3-dB bandwidth according to Eq. (23).

where $G$ is the signal power gain. From Eq. (22) we can extract $\beta_{AB}$ needed to get the desired gain, for example, a 20-dB gain will require $|\beta_{AB}| = 0.452$.

For high gain and small detuning, Eq. (21) approximates a Lorentzian whose bandwidth is

$$\Delta\omega = \frac{2}{\sqrt{G}}\frac{\gamma_A\gamma_B}{\gamma_A + \gamma_B}, \qquad (23)$$

which is maximal when $\gamma_A = \gamma_B$, and inversely proportional to the amplitude gain.

The two driven modes of the parametric amplifier are often identified as *signal* and *idler*. This terminology is anchored in historical jargon—early nondegenerate parametric amplifiers terminated the idler tank circuit (i.e., the resonator that did not host the incident signal mode) [40,41]. The idler circuit provides a critical internal degree of freedom necessary for amplification, but might have been historically viewed as an ancillary mode.

Figure 4 shows the signal ($S_{AA}$) and idler ($S_{BA}$) gain profiles of an amplifier pumped with the $\beta_{AB}$ we calculated above to give $G = 20$ dB at $\omega_0/2\pi = 5$ GHz, and with $\gamma_A/2\pi = \gamma_B/2\pi = 600$ MHz. The arrows indicate the 3-dB bandwidth calculated using Eq. (23), 60 MHz in this case. The bandwidth of the amplifier can be increased rather dramatically by embedding the two-mode primitive of Fig. 2(c) in a passive matching network [5–7,42,43]. Section V D shows how to engineer these matching networks to obtain prescribed gain characteristics.

### 3. Parametric circulator

The parametric converter and parametric amplifier are represented by simply connected graphs (there are no loops) and therefore the phase of the pump only adds an overall phase in the $S$ parameters but otherwise does not affect the behavior of the device. Therefore, in the examples above we could have taken the coupling terms to
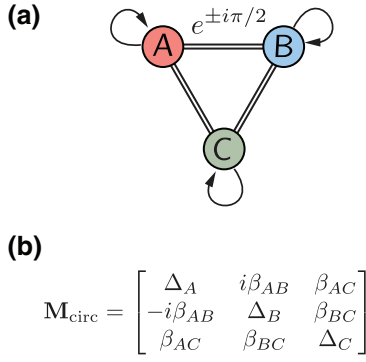
**(a)**



**(b)**

$$\mathbf{M}_{\text{circ}} = \begin{bmatrix} \Delta_A & i\beta_{AB} & \beta_{AC} \\ -i\beta_{AB} & \Delta_B & \beta_{BC} \\ \beta_{AC} & \beta_{BC} & \Delta_C \end{bmatrix}$$

FIG. 5. (a) Coupling graph of a three-mode parametric circulator, indicating the relative pump phase, $\pm\pi/2$, of the $A$-$B$ edge. (b) Corresponding equation-of-motion matrix for a pump phase of $\pi/2$.



FIG. 6. $S$ parameters of the three-mode parametric circulator, calculated using Eq. (8). The frequency axis is referenced to the signal port $A$.

be real without loss of generality. When the network's graph is multiply connected, the relative phases of the coupling terms matter. The (anti)conjugate symmetry of the parametric coupling coefficients, combined with interference from closed loops in these geometries, can generate synthetic nonreciprocal scattering [18].

Figure 5(a) shows the coupled-mode graph of the three-mode circulator [9], one of the simplest devices to implement parametric nonreciprocity. The device has three resonant modes, coupled pairwise with parametric conversion processes (difference-frequency pumps), where one of the couplings (the $A$-$B$ edge in Fig. 5) carries a phase of $\pm\pi/2$ to affect circulation, and the circulation direction depends on the sign of that phase. In the figure, the modes are colored to represent three different mode frequencies; note, however, that the minimal construction would require only mode $B$ to be parametrically coupled and thus at a different frequency, while modes $A$ and $C$ can have the same frequency with a passive coupling between them.

Figure 5(b) shows the equation-of-motion matrix where we have included the $\pi/2$ phase of the $A$-$B$ edge ($i\beta_{AB}$ in the upper triangle of the matrix, explicitly factoring out the phase so that $\beta_{AB}$ is real) and used the conjugation rule in Fig. 1 to write $\beta_{BA} = -i\beta_{AB}$ in the lower triangle. All other couplings are assumed to be real.

If the port coupling is equal for all ports, $\gamma_A = \gamma_B = \gamma_C = \gamma_0$, then from Eq. (8) we see that the condition for perfect isolation from port $C$ to port $A$ at zero detuning, $S_{AC}(\omega_A^s = \omega_A) = 0$, requires $\beta_{AB}\beta_{BC} = \beta_{AC}/2$, and similarly isolation from port $A$ to port $B$, $S_{BA} = 0$, requires $\beta_{AB}\beta_{AC} = \beta_{BC}/2$. These two conditions give $\beta_{AB} = \beta_{BC} = \beta_{AC} = 0.5$. This set of parameters also results in a match at each of the ports at zero detuning, e.g., $S_{AA}(\omega_A^s = \omega_A) = 0$.

Figure 6 shows the $S$ parameters calculated using Eq. (8) and the coupling matrix of Fig. 5(b), with all port couplings set to $\gamma_0/2\pi = 400$ MHz, and with all the $\beta$ equal to 0.5. At the center frequency of the device we get unity
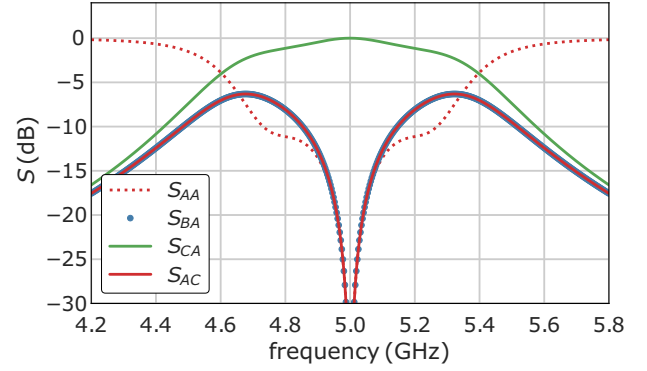
conversion ($S_{CA}$; green line) of signals entering port $A$ near $\omega_A$ to signals leaving port $C$ near $\omega_C$, while in the backwards direction [from $A$ to $B$, $S_{BA}$ (blue circles), or from $C$ to $A$, $S_{AC}$ (red solid line)] we get zero conversion. In addition, all ports are matched (e.g., $S_{AA}$; red dotted line), as is the case for an ideal circulator.

### D. Graph reduction

The graph of a coupled-mode system can be simplified by eliminating nodes from the graph, in a process known as Kron reduction [44]. The edges and self-loops of any remaining node that was previously connected to the eliminated node will be rescaled to account for change in the connectivity of the graph. When a node $k$ is eliminated, the new, resulting graph is represented by a new equation-of-motion matrix $\mathbf{M}'$, such that the new matrix components can be calculated from those of the old matrix $\mathbf{M}$ via [13] (no summation implied)

$$M'_{ij} = M_{ij} - \frac{M_{ik}M_{kj}}{M_{kk}}. \tag{24}$$

For example, referring to the parametric converter in Fig. 2(b), if we are only interested in the reflection off of mode $A$, we can eliminate mode $B$ from the graph—in this case the resulting graph will have only one mode, and the equation-of-motion matrix reduces to a single element $\Delta'_A$:

$$\Delta'_A = M'_{AA} = M_{AA} - \frac{M_{AB}M_{BA}}{M_{BB}} = \Delta_A - \frac{|\beta_{AB}|^2}{\Delta_B}. \tag{25}$$

For the purpose of driving toward our main goal in this tutorial, we are interested in the admittance seen at a certain port, and we use graph reduction to write Eq. (12) in the form

$$\frac{Y_k}{Y_0} = -2i\frac{\gamma_0}{\gamma_k}\Delta'_k - 1, \tag{26}$$

FIG. 7.   Graph reduction of a four-mode circuit with nearest-neighbor connectivity, where couplings are either passive or via parametric frequency conversion processes.

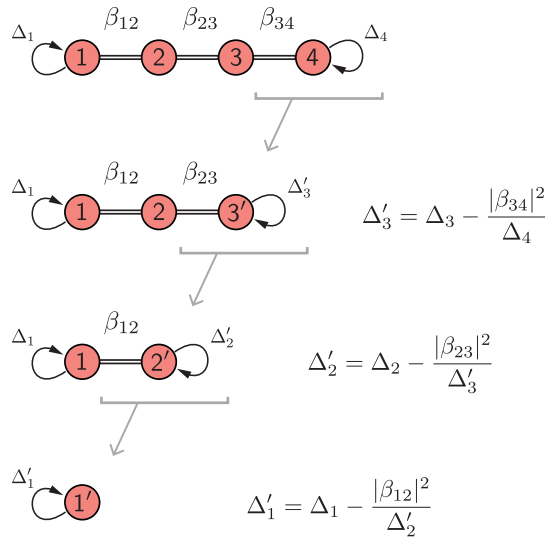where $\Delta_k'$ is the overall result of successively applying Eq. (24) to eliminate all other modes, as shown for the one-dimensional (1D) nearest-neighbor coupled four-mode circuit in Fig. 7.

Carrying out the successive substitutions as indicated in Fig. 7, we can write

$$\Delta_1' = \Delta_1 - \cfrac{|\beta_{12}|^2}{\Delta_2 - \cfrac{|\beta_{23}|^2}{\Delta_3 - \cfrac{|\beta_{34}|^2}{\Delta_4}}}. \qquad (27)$$

Note that the dissipation due to the port connected to mode 4 in Fig. 7 is embedded in Eq. (27) via its dependence on $\Delta_4$. Therefore, $\Delta_1'$ will have an effective "internal" dissipation included in its nonvanishing imaginary part.

The pattern that emerges from Eqs. (26) and (27) is that the admittance function of a 1D-connected graph can be written as a continued-fraction expression, where each of the terms is linear in signal frequency. Recall (Sec. II C) that, for parametric processes under a resonant pump condition, the different frequencies of the modes all get projected to the signal band, and all detuning terms will have the same frequency dependence $\propto (\omega - \omega_0)$.

In Appendix F we show that the continued fraction expression of Eq. (27) can be used to write the admittance in Cauer form [45], which is used in network synthesis to extract the network's normalized low-pass prototype coefficients.

## III. PARAMETRIC COUPLING AS A CIRCUIT ELEMENT

In the previous section we developed implementation-agnostic methods to analyze parametrically coupled circuits using the coupling matrix formalism [18]. To bring the discussion down to the device level, we next examine how we can understand parametric couplings as functional circuit elements. We develop this understanding by considering a sinusoidally modulated inductance in a microwave circuit. This model is a generalization of parametrically modulated elements that are commonly used today, including single Josephson junctions, superconducting quantum interference devices (SQUIDs) (see Appendix B), and kinetic inductance-based implementations [46]. The discussion here is inspired by much earlier work on modulated capacitors (varactors) [47].

We consider an inductor whose value is sinusoidally modulated, $L(t) = L_0 + |\delta L| \cos \omega_P t$, as shown in Fig. 8(a). The modulated inductor may be embedded in a microwave circuit as shown in the figure, and can participate in the total inductance that defines one or more $LC$ resonators. If this element carries two branch currents, $I_1$ and $I_2$, oscillating at two different frequencies, the voltage across this modulated inductor is

$$\begin{aligned}
V(t) &= \frac{d\Phi(t)}{dt} \\
&= \frac{d}{dt}\Bigg[\left(L_0 + \frac{\delta L e^{j\omega_P t} + \delta L^* e^{-j\omega_P t}}{2}\right) \\
&\quad \times \sum_{k=1,2} \frac{I_k e^{j\omega_k t} + I_k^* e^{-j\omega_k t}}{2}\Bigg].
\end{aligned} \qquad (28)$$

We can identify signals oscillating at $\pm\omega_1$ as the *signal*, and those oscillating at $\pm\omega_2$ as the *idler* [1]. We assume that the circuit embedding the modulated inductor is designed such that oscillations at any other frequency are effectively "shorted out," i.e., $V_k = 0$ for $k \notin \{1, 2\}$, and we can therefore ignore other mixing products [23]. In physics jargon, elimination of these other modes is a form of *rotating wave approximation*. In nondegenerate amplifier and frequency conversion circuits, we further assume same-frequency isolation between the signal and idler circuits, meaning that the idler network presents an open circuit (in shunt representation) or short circuit (in series representation) at the signal frequency, and vice versa. Below, we take the convention that all frequencies $\omega_k > 0$ and $\omega_2 > \omega_1$.

If the pump is driven at $\omega_{P,\mathrm{FC}} = \omega_2 - \omega_1$, we couple the voltage and current components oscillating at $\omega_1$ to those oscillating at $\omega_2$, corresponding to a parametric frequency conversion process. If the pump frequency alternatively satisfies $\omega_{P,\mathrm{PA}} = \omega_1 + \omega_2$, we couple components oscillating at $\omega_1$ to those at $-\omega_2$, corresponding to
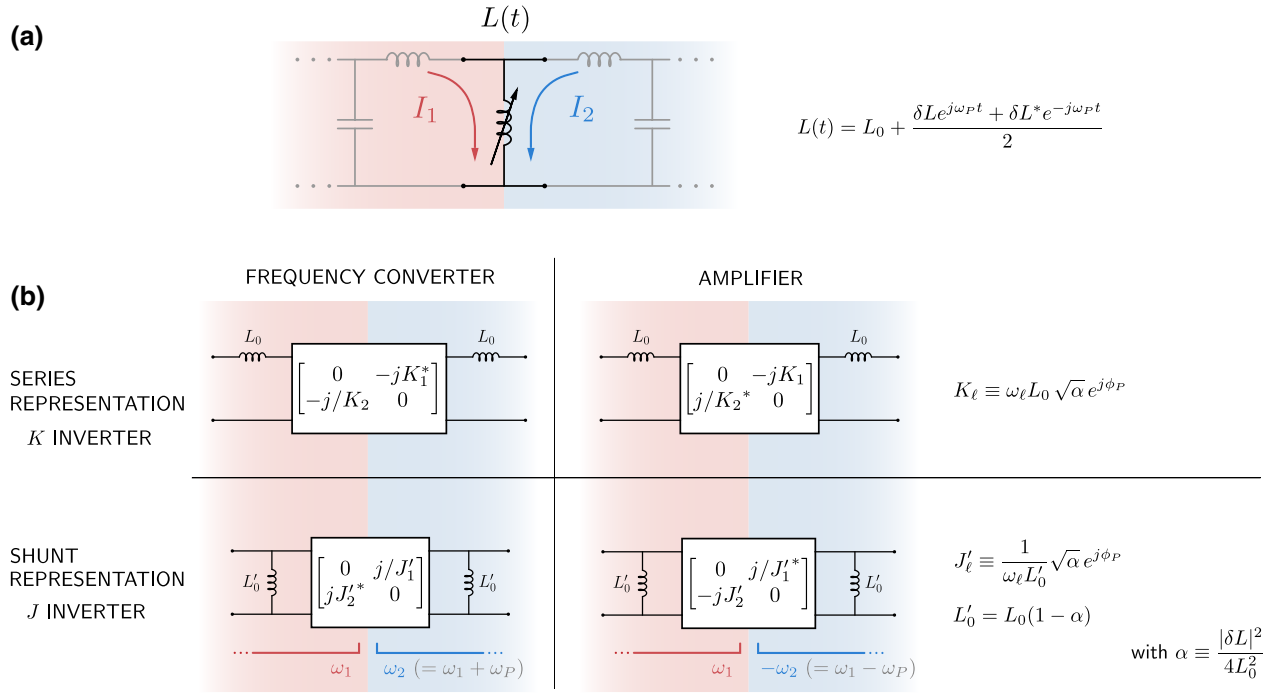
FIG. 8. (a) Modulated inductor model with signal and idler branch currents $I_1$ and $I_2$. An example embedding circuit is shown (grayed out) to provide context. (b) Equivalent two-port circuit models for the *series* and *shunt representations* of the modulated inductor. The boxed elements represent impedance or admittance inverters, with the corresponding *ABCD* matrices shown. The constants $K_\ell$, $J'_\ell$, and $L'_0$ are defined in the figure.

a parametric amplification process. When $\omega_1 \neq \omega_2$ (non-degenerate parametric amplification), we get additional frequency conversion.

### A. Parametric conversion

When the inductance in Fig. 8(a) is pumped at the difference frequency, $\omega_{P,\mathrm{FC}} = \omega_2 - \omega_1$, only those voltage components that oscillate at $\omega_1$ and $\omega_2$ survive in Eq. (29). We can therefore write

$$V_1 = j\omega_1 L_0 I_1 + j\omega_1 \frac{\delta L^*}{2} I_2, \tag{29}$$

$$V_2 = j\omega_2 \frac{\delta L}{2} I_1 + j\omega_2 L_0 I_2, \tag{30}$$

yielding the following impedance $Z$ matrix [28]:

$$\mathbf{Z}_{L,\mathrm{FC}} = \begin{bmatrix} j\omega_1 L_0 & j\omega_1 \delta L^*/2 \\ j\omega_2 \delta L/2 & j\omega_2 L_0 \end{bmatrix}. \tag{31}$$

The $Z$ matrix (or its inverse, the admittance $Y$ matrix) can be converted to an *ABCD* (transmission) matrix [28] (see Appendix A), and the linear time-independent part of the inductance can be factored out as shown in Fig. 8(b). The remaining, purely parametric, part of the frequency

converter *ABCD* matrix in a series representation becomes

$$\mathbf{T}_{\mathrm{FC}} = \begin{bmatrix} 0 & -jK_1^* \\ -j/K_2 & 0 \end{bmatrix}, \tag{32}$$

where $K_\ell$ is defined in Fig. 8(b).

### B. Parametric frequency conversion is a generalized impedance or admittance inverter

What functional role does an element described by the *ABCD* matrix in Eq. (32) play in a circuit? Calculating the impedance $Z_1(\omega_1) = V_1/I_1$ seen from the circuit's input when its output port is terminated with an impedance $Z_2(\omega_2) = V_2/I_2$ we get

$$Z_1(\omega_1) = \frac{K_1^* K_2}{Z_2(\omega_2)}. \tag{33}$$

Microwave engineers will recognize the function of the parametric coupling, as embodied in Eq. (33), as an impedance ($K$) inverter [48]—the canonical example in passive circuits is the quarter-wave transformer with impedance $Z_{\lambda/4} = K$, which transforms a load $Z_L$ into an input impedance $Z_{\mathrm{in}} = Z_{\lambda/4}^2/Z_L$ [28]. Similarly, the shunt representation in Fig. 8(b) functions as an admittance ($J$) inverter, transforming admittances according to $Y_1 = J_1'^* J_2'/Y_2$.

A key insight of this tutorial is that a parametric coupling driven with a difference-frequency pump generalizes the concept of the passive impedance (admittance) inverter, in that it transforms between impedances connected to ports that are not necessarily at the same frequency [42,43]. Additionally, the parametric impedance inverter $K$ can be complex, meaning that it carries information about the phase of the pump. Although one can view the modulated inductor as a cross-frequency inverter as we have shown here, it is important to understand this element as physically generating the mode coupling rates $c_{jk}$ in our general coupled-mode picture. The inverter constants can be directly related to the normalized coupling rates

$$|\beta_{12}|^2 = \frac{1}{\gamma_0^2}\frac{K_1^* K_2}{L_1 L_2} = \frac{1}{\gamma_0^2}\frac{\omega_1\omega_2|\delta L|^2}{4L_1 L_2},\qquad(34)$$

where $L_1$ and $L_2$ are the total effective inductances (including $L_0$) of the two coupled modes [40]; see Fig. 8(a).

Passive impedance or admittance inverters (collectively referred to as "immittance" inverters in electrical engineering) are used extensively in microwave engineering as a tool to construct impedance-matching and filter networks [48]. We discuss inverters and their use in Sec. IV. The close functional similarity they share with parametric conversion processes invites the designer of parametrically coupled devices to borrow techniques and methodologies from the existing, vast body of knowledge on filter network design. In return, the additional characteristics of parametric couplers, such as the complex phase, can expand the palette available to the filter network designer to encompass new features such as synthetic nonreciprocity.

### C. Parametric amplification

When the inductance in Fig. 8(a) is pumped at the sum frequency, $\omega_{P,\mathrm{PA}} = \omega_1 + \omega_2$, Eq. (29) reduces to

$$V_1 = j\omega_1 L_0 I_1 + j\omega_1\frac{\delta L}{2}I_2^*,\qquad(35)$$

$$V_2^* = -j\omega_2\frac{\delta L^*}{2}I_1 - j\omega_2 L_0 I_2^*,\qquad(36)$$

and can be described by the $Z$ matrix

$$\mathbf{Z}_{L,\mathrm{PA}} = \begin{bmatrix} j\omega_1 L_0 & j\omega_1\delta L/2, \\ -j\omega_2\delta L^*/2 & -j\omega_2 L_0 \end{bmatrix}.\qquad(37)$$

From the resulting *ABCD* matrix [Fig. 8(b) and Appendix A] we see that, in the series representation, the parametric amplification process transforms impedances

according to

$$Z_1(\omega_1) = -\frac{K_1' K_2'^*}{Z_2^*(\omega_2)},\qquad(38)$$

and, in the shunt representation, admittances are transformed according to

$$Y_1(\omega_1) = -\frac{J_1'^* J_2'}{Y_2^*(\omega_2)}.\qquad(39)$$

Equations (38) and (39) suggest that the parametric amplification process functions as an "anticonjugating" immittance inverter, to which there is no passive analogue. The negative sign in Eq. (38) indicates that the input port is presented with an effective impedance whose real part is negative, resulting in gain. A useful concept for practical design is the so-called "pumpistor model" introduced in Ref. [49], where the input admittance, $Y_{\mathrm{in}}$, presented to the signal circuit at the terminals of the modulated inductor relates to admittance of the idler circuit as transformed via this anticonjugating inverter. Using the shunt representation of Fig. 8(b) and definitions therein, this can be written as

$$Y_{\mathrm{in}}(\omega_1) = \frac{1}{j\omega_1 L_0'}\left[1 + \frac{\alpha}{j\omega_2 L_0' Y_{\mathrm{idler}}^*(\omega_2) - 1}\right],\qquad(40)$$

where $Y_{\mathrm{idler}}$ is the admittance of the idler circuit. Equation (40) is equivalent to the "pumpistor" admittance derived in Ref. [49], and models the modulated inductor as an inductance in parallel with a negative resistance.

A relation similar to Eq. (34), relating the inductance modulation strength to the coupling rate in the coupled-mode picture, can be derived from the discussion in Sec. V D 3, and is given in Appendix C.

### D. Modulated mutual coupling

Above we discussed a particular circuit implementation of a parametric coupler, namely, the grounded modulated inductor, which can be implemented by a Josephson junction or a dc SQUID (Appendix B). We note however that the same reasoning can be applied to other types of parametric couplers, for example, signal and idler circuits that are coupled via a modulated mutual inductance, as was shown in Fig. 2(a):

$$M(t) = M_0 + \delta M\cos(\omega_P t).\qquad(41)$$

This model is more appropriate for circuits like the JPC [39], the rf-SQUID coupler [50–52], or even dispersive couplers [53]. These types of couplers may be advantageous over the grounded SQUID in that they allow nulling of the passive part of the coupling, $M_0 = 0$, providing same-frequency isolation between the idler and signal circuits, and making the coupling purely parametric.
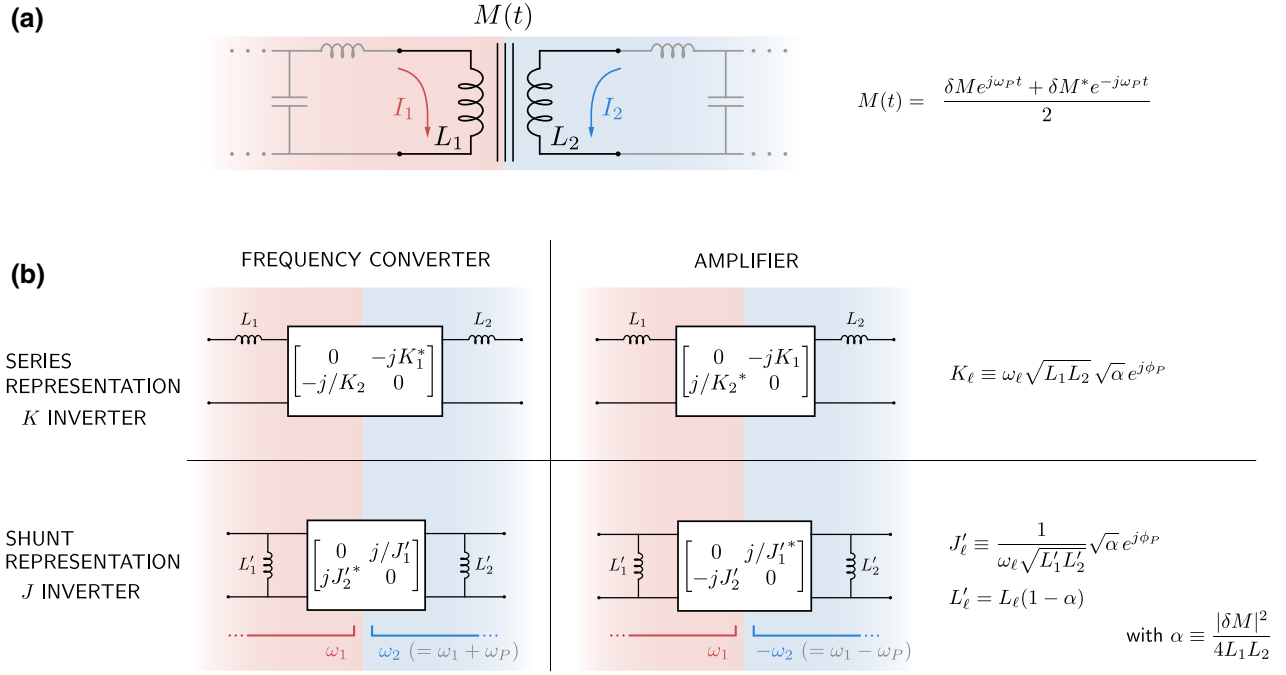
FIG. 9. (a) Modulated mutual inductance model with signal and idler branch currents $I_1$ and $I_2$. An example embedding circuit is shown (grayed out) to provide context. (b) Equivalent two-port circuit models for the *series* and *shunt representations* of the modulated mutual. The boxed elements represent impedance or admittance inverters, with the corresponding *ABCD* matrices shown. The constants $K_\ell$, $J'_\ell$, and $L'_\ell$ are defined in the figure.

For a circuit having a signal inductor $L_1$ and an idler inductor $L_2$, which are coupled by the modulated mutual inductance of Eq. (41), and where $M_0$ is nulled [Fig. 9(a)], we can write the $Z$ matrices coupling currents and voltages oscillating at $\omega_1$ and $\omega_2$ as

$$\mathbf{Z}_{M,\mathrm{FC}} = \begin{bmatrix} j\omega_1 L_1 & j\omega_1 \delta M^*/2 \\ j\omega_2 \delta M/2 & j\omega_2 L_2 \end{bmatrix} \qquad (42)$$

and

$$\mathbf{Z}_{M,\mathrm{PA}} = \begin{bmatrix} j\omega_1 L_1 & j\omega_1 \delta M/2 \\ -j\omega_2 \delta M^*/2 & -j\omega_2 L_2 \end{bmatrix}. \qquad (43)$$

Comparison with Eqs. (31) and (37) indicates that this can be considered a generalization of the modulated inductor model with $L_1 = L_2 = L_0$ and, likewise, one can think of the inductance modulation amplitude $\delta L$ as corresponding to a modulated mutual inductance. The equivalent transmission matrices and inverter constant definitions are summarized in Fig. 9(b).

## IV. BAND-PASS IMPEDANCE MATCHING AND FILTER NETWORKS

Up to this point we have outlined a graph-based language that facilitates rapid analysis of arbitrary, linearly coupled mode systems, including a direct mapping between scattering parameters and the collections

of coupling permutations that generate them. We have seen hints in Secs. II C and II D that point to a deeper connection between parametric coupled-mode network design and the problem of filter and matching network design known from microwave engineering. In fact, similar graph-based approaches are already established in the design of microwave frequency cavity-based filters [54] and photonic circuits [55]. Furthermore, in Sec. III we saw that parametric couplings serve a similar circuit function to that of immittance inverters in microwave filter networks. Before we detail in Sec. V an exact correspondence between the language of coupled-mode theory and that of filter design, we review here a few key concepts from microwave band-pass network synthesis. Filter synthesis techniques are already a very mature topic within electrical engineering [28,56,57], so we will keep the discussion here to the minimum necessary to provide a foundation for Sec. V. Appendix E gives a more detailed explanation of how network prototype coefficients are calculated.

Band pass filter design begins by selecting a target transmission profile (e.g., ripple and roll-off characteristics), from which we can choose the desired number of filter sections $N$, the filter's center frequency $\omega_0$, bandwidth $\Delta\omega$, and response type (Chebyshev, Butterworth, etc.). We find the corresponding normalized filter coefficients $\{g_i\}$ from tables in, e.g., Refs. [28,57], where for an $N$ section filter, we have $N + 2$ zero-indexed coefficients. These coefficients relate to polynomials specifying the
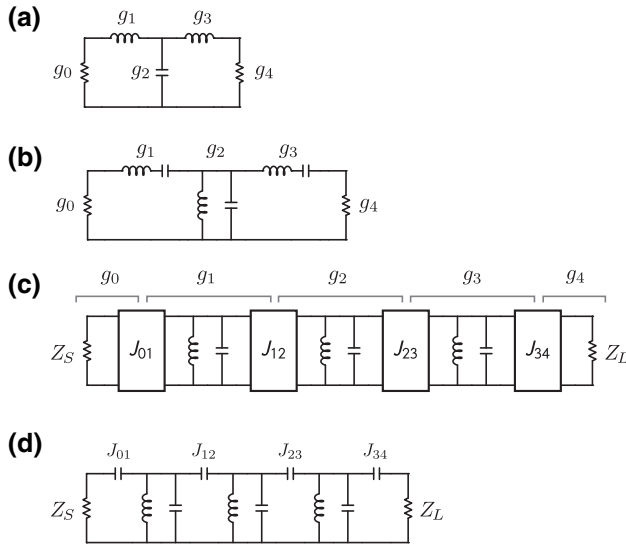
**(a)**



**(b)**

**(c)**

**(d)**

FIG. 10.   Example of three-pole band-pass network construction. (a) Low-pass prototype, (b) band-pass transformation, (c) added admittance inverters, and (d) inverters implemented.

input impedance of the network as a function of frequency (Appendix E). The coefficient $g_0$, representing the conductance of the source, is often omitted from tables as usually $g_0 = 1$ by definition. The last coefficient, $g_{N+1}$, represents the conductance of the load. The remaining coefficients $g_1, \ldots, g_N$ correspond to the normalized reactances of the elements (alternating capacitors and inductors) that make up the low-pass filter prototype, as in Fig. 10(a).

### A. Series/shunt band-pass ladder network design

Students are usually taught to start with a low-pass prototype network, Fig. 10(a), then convert each of the reactances to a resonant circuit via a band-pass transformation [28]. The result is a coupled-resonator circuit, Fig. 10(b), that alternates between shunt-connected parallel-$LC$ resonators and series-connected series $LC$ resonators.

For a given set of prototype coefficients $\{g_i\}$, a specified reference impedance $Z_0 = 1/Y_0$, and a specified center frequency $\omega_0$ and bandwidth $\Delta\omega$, the resonators should be constructed such that the admittance $Y_j$ of the parallel resonator corresponding to the prototype coefficient $g_j$ is given by

$$Y_j = g_j \frac{\omega_0}{\Delta\omega} Y_0, \tag{44}$$

and the impedance $Z_k$ of the series resonator corresponding to the prototype coefficient $g_k$ is

$$Z_k = g_k \frac{\omega_0}{\Delta\omega} Z_0. \tag{45}$$

The last coefficient, $g_{N+1}$, corresponds to the load immittance, and its denormalization will depend on whether it is

preceded by a series section or a parallel section:

$$Z_L = \begin{cases} \dfrac{Z_0}{g_{N+1}}, & N\text{th section series,} \\ Z_0 \times g_{N+1}, & N\text{th section parallel.} \end{cases} \tag{46}$$

Once the resonator impedances $Z_i$ are known, their inductances and capacitances can be calculated in the usual way, $L_i = Z_i/\omega_0$ and $C_i = 1/Z_i\omega_0$. The coupling rate between the $j$ parallel resonator and the neighboring $k = j \pm 1$ series resonator is a function of their respective impedances:

$$c_{jk} = \omega_0 \sqrt{\frac{Z_j}{Z_k}}. \tag{47}$$

This method of circuit construction will be useful in understanding the results of Ref. [6], as we show in Sec. V D 2.

### B. Coupled-resonator method for band-pass network design

The series/shunt ladder network we get by following the procedure in Sec. IV A may be difficult to implement in practice, as it offers little flexibility in component selection, and does not generalize well to circuits that are not based on lumped-element electrical resonators. A more convenient circuit can be realized by replacing the series-connected series-$LC$ resonators with shunt-connected parallel-$LC$ resonators sandwiched between two admittance inverters [48], $J_{jk}$, as shown in Fig. 10(c). In this configuration, the inverters are responsible for the coupling between the resonators. Because the inverters can also transform between impedance levels, the designer is now free to choose the resonator impedances to best fit the available technology. This circuit topology of coupled resonators additionally lends itself more naturally to a description based on the coupled-mode language developed in Sec. II.

Coupled-resonator band-pass network design methods are illustrated in detail in Ref. [57]. Start with a set of $N + 2$ prototype coefficients $\{g_j\}$ for a network of $N$ resonators having a resonance frequency $\omega_0$ and impedances $Z_j$, $j = 1, \ldots, N$. To implement a network with a fractional bandwidth $w = \Delta\omega/\omega_0$ that operates between a source impedance $Z_S$ and a load impedance $Z_L$, and is based on lumped-element shunt-$LC$ resonators, calculate the values $J_{jk}$ of the admittance inverters [57]:

$$J_{01} = \sqrt{\frac{w}{g_0 g_1 Z_S Z_1}}, \tag{48}$$

$$J_{jk} = \frac{w}{\sqrt{g_j g_k Z_j Z_k}}, \tag{49}$$

**(a)**



$$L_{jk} = \frac{1}{\omega_0 J_{jk}}$$

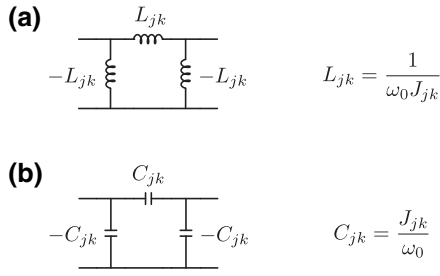**(b)**



$$C_{jk} = \frac{J_{jk}}{\omega_0}$$

FIG. 11. Lumped-element physical implementations of an admittance inverter, using (a) an inductive $\pi$ section and (b) a capacitive $\pi$ section.

$$J_{N,N+1} = \sqrt{\frac{w}{g_N g_{N+1} Z_N Z_L}}. \qquad (50)$$

Next, choose a physical implementation for each of the inverters; in a lumped-element circuit we can choose either the inductive circuit of Fig. 11(a) or the capacitive circuit of Fig. 11(b), and calculate the inductance or capacitance of the inverter based on the corresponding $J$ value, i.e., $C_{jk} = J_{jk}/\omega_0$ and $L_{jk} = 1/\omega_0 J_{jk}$. The negative values of the shunt components in Fig. 11 will be absorbed by the neighboring resonators when the inverter is incorporated into the circuit. The resulting circuit will have the general structure as Fig. 10(d) in which capacitive inverters were used. Since the source (load) resistor cannot absorb a negative reactance associated with the first (last) inverter, we have to modify their component values as outlined in Appendix D and Ref. [57]. Finally, calculate $L$ and $C$ of the shunt resonators using $\omega_0$, their respective impedances, and the absorbed inverter component values.

The physical implementation of immittance inverters, as in Fig. 11, is always associated with the additional frequency dependence of the inverter itself. For this reason, the methods described herein are typically suitable for designs with fractional bandwidth up to approximately 20%. Techniques for designs with higher bandwidth can be found in, e.g., Ref. [57].

We illustrated the coupled-resonator design method here with lumped-element parallel-$LC$ resonators coupled by admittance inverters. If the preferred resonator type is a series $LC$, a similar procedure that uses impedance ($K$) inverters can be used [48,57]. Ref. [57] additionally details expressions similar to Eqs. (48)–(50) for implementations based on half- and quarter-wave transmission line resonators. A practical design example is given in Sec. IV D.

### C. Impedance matching of a resonated load

We already mentioned that the use of immittance inverters in a filter design offers flexibility in choosing the impedance levels of the constituent resonators. Indeed, it is clear from Eqs. (48) and (50) that the design can also accommodate arbitrary source and load impedances, so that networks designed using the coupled-resonator method can conveniently serve as impedance-matching networks.

In many cases that will be important to our discussion here, we will have to design band-pass networks to match a given "resonated load"—essentially a resistance shunted by an $LC$ resonator, or more generally, some admittance function $Y(\omega)$ that can be approximated by an $LC$ resonator with a finite quality factor $Q$ at a particular frequency of interest. The latter is a case that we encounter in Sec. V C when matching a parametric circulator. In the case of Josephson parametric amplifiers (Sec. V D), we will be presented with the need to match a load (the parametrically pumped SQUID) that looks like a (negative) resistance in parallel with an inductance; we "resonate" this load by adding a shunt capacitor to the device.

The $Q$ factor of the resonated load can be calculated from its admittance $Y(\omega)$ via [57]

$$Q = \frac{\omega_0}{2\text{Re}\{Y(\omega_0)\}} \frac{d}{d\omega} \text{Im}\{Y(\omega)\}\Big|_{\omega=\omega_0}, \qquad (51)$$

where $\omega_0$ is the resonance frequency. For a resistor $R$ shunted by a parallel lumped $LC$ resonator with impedance $Z_{\text{res}}$, this reduces to the usual $Q = R/Z_{\text{res}}$.

Once the $Q$ factor is known, we can proceed with the network design, with the resonated load accounting for the elements labeled as $g_0$ and $g_1$ in Fig. 10(c). The network bandwidth will be constrained by the so-called "decrement" relation [57]

$$w = \frac{g_0 g_1}{Q}, \qquad (52)$$

where here, too, $w$ is the fractional bandwidth.

Equation (52) means that if we have a bandwidth requirement to satisfy, we can find the required impedance for the resonator embedding the load. If, instead, we have a given resonator but the load resistance may be adjustable (e.g., via its dependence on a parametric pump amplitude; cf. Section V D 3), then Eq. (52) lets us set that control knob [7]. If $Q$ of the resonated load is fixed then we have to design the rest of the network to have the same bandwidth $w$ given by Eq. (52).

Note that the decrement condition, Eq. (52), is synonymous to requiring a transformation of the reference admittance $Y_0 = 1/Z_0$ through the inverter $J_{01}$ specified by the network prototype, i.e.,

$$\text{Re}\{Y(\omega_0)\} = \frac{J_{01}^2}{Y_0}.$$

### D. Coupled-resonator filter design example

As an example, we design a three-pole, 500-MHz bandpass filter centered at $\omega_0/2\pi = 5$ GHz using a 0.5-dB ripple Chebyshev prototype, in a $Z_0 = 50\ \Omega$ environment.

The prototype coefficients for a three-pole, 0.5-dB ripple Chebyshev network can be found in, e.g., Ref. [28]: $g_i = \{1.0, 1.5963, 1.0967, 1.5963, 1.0\}$. We choose (rather arbitrarily for demonstration purposes) the impedances of the three resonators, highlighted in Fig. 12(a), to be $Z_1 = 40\ \Omega$, $Z_2 = 30\ \Omega$, and $Z_3 = 40\ \Omega$.

We implement the admittance inverters using capacitive $\pi$ sections, as in Fig. 11(b). Using Eqs. (48)–(50), and the required fractional bandwidth of $w = 0.1$, we calculate the inverter values: $J_{01} = J_{34} = 0.0056\ \Omega^{-1}$ and $J_{12} = J_{23} = 0.0022\ \Omega^{-1}$. From here, the coupling capacitances of the "internal" inverters $C_{jk} = J_{jk}/\omega_0$ can be evaluated [refer to the schematic in Fig. 12(a)], $C_{12} = C_{23} = 0.069$ pF. For the "external" inverters that couple the filter to the source and load (see Appendix D), we use the relations [57]

$$C_{01} = \frac{J_{01}}{\omega_0\sqrt{1 - (Z_0 J_{01})^2}}, \qquad (53)$$

$$C_{34} = \frac{J_{34}}{\omega_0\sqrt{1 - (Z_0 J_{34})^2}} \qquad (54)$$

to get $C_{01} = C_{34} = 0.186$ pF.

The values of the inductance $L_j$ of resonator $Z_j$ are simply calculated using $L_j = Z_j/\omega_0$: $L_1 = L_3 = 1.27$ nH and $L_2 = 0.96$ nH. The resonator capacitors have to absorb the



**(a)**

**(b)**

FIG. 12. Three-pole filter design example. (a) Circuit schematic, (b) $S$-parameter simulation in Keysight ADS.

negative shunt capacitances of the inverters, so that

$$C_1 = \frac{1}{Z_1\omega_0} - C_{01e} - C_{12} = 0.56\ \text{pF}, \qquad (55)$$

$$C_2 = \frac{1}{Z_2\omega_0} - C_{12} - C_{23} = 0.92\ \text{pF}, \qquad (56)$$

$$C_3 = \frac{1}{Z_3\omega_0} - C_{23} - C_{34e} = 0.56\ \text{pF}, \qquad (57)$$

where we have used [Appendix D, Eq. (D2), and Ref. [57]] $C_{01e} = (J_{01}/\omega_0)\sqrt{1 - (Z_0 J_{01})^2}$, and similarly for $C_{34e}$.

Now that all component values are specified, we can construct the circuit in Fig. 12(a) and simulate its response. An $S$-parameter simulation using Keysight ADS is shown in Fig. 12(b), showing that the center frequency, bandwidth, and ripple requirements are met. The slight asymmetry seen in the response is due to the additional frequency dependence introduced by the physical implementation of the admittance inverters as capacitive networks.

### E. Filter synthesis methodically determines resonator coupling rates

The preceding sections, and the example in Sec. IV D, demonstrate that band-pass filter synthesis boils down to determining the values of the immittance inverters that are disposed between the filter resonators, and between the resonators and the environment. We have seen that these structures effectively control the coupling rates in the circuit, as their physical implementation as coupling capacitors or inductors would suggest.

A third key insight in this tutorial is that the art of band-pass network synthesis is concerned with methodically engineering the coupling rates in a system of resonant modes. These methods transcend electrical circuit design and could be applied in diverse areas such as mechanical [58], acoustic [59], or optical [55,60] filter design.

## V. ENGINEERING COUPLED-MODE NETWORKS

The discussion thus far points toward a deep connection between parametric networks and filter networks. Here, we build on the insights developed in the preceding sections to unify the language used to describe these systems.

A key insight from Sec. II C is that in parametric networks that are driven by pumps that are tuned to either the sum or the difference frequency, the fact that the different modes in the circuit have different frequencies essentially drops out of the equations—the behavior of the circuit can be described using a single reference frequency, usually taken as that of the signal mode. In that respect, the equation-of-motion matrices of systems coupled via parametric conversion processes with 1D connectivity are indistinguishable (up to an overall phase) from
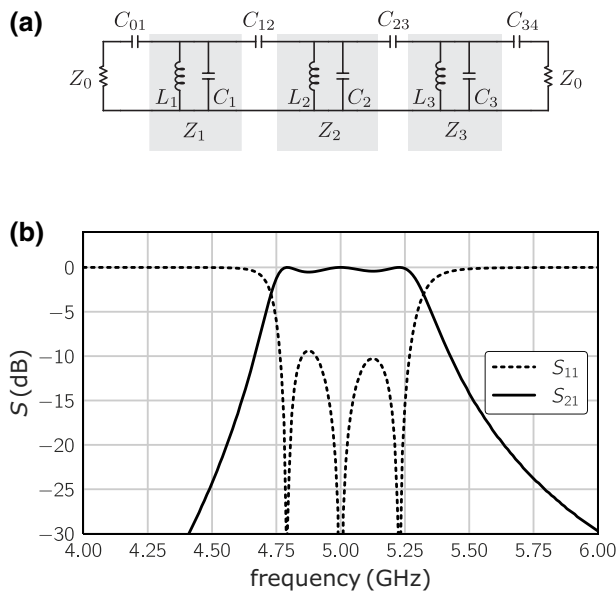
those of passively coupled circuits such as band-pass filters. The novelty of parametric coupling only manifests in the off-diagonal elements of the equation-of-motion matrix, through nontrivial phases (in the case of multiply connected circuits) and anticonjugation (in the case of parametric amplification).

The second key insight, arising from Sec. III, is that parametric couplings function as generalized immittance inverters. The use of immittance inverters in the design of filter networks was described in Sec. IV, where we developed an additional insight, that the art of filter synthesis is ultimately concerned with methodically determining coupling rates between resonant modes in the circuit. Immittance inverters should therefore be thought of as the circuit implementation of the off-diagonal elements in the coupled-mode equation-of-motion matrices of Sec. II.

### A. Correspondence of coupled-mode and filter networks

Figure 13 displays, side by side, a four-mode graph of a coupled-mode system and a fourth-order band-pass electrical network. This graph can represent, for example, an $N$-stage transduction network [61,62], a multimode parametric converter, or matched parametric amplifier [7]. Each of the nodes in the graph corresponds to an $LC$ resonator in the filter network, and the ports—indicated by the self-loops in the graph—correspond to the source and load resistors of the electrical circuit. The graph edges $\beta_{jk}$ (which represent the off-diagonal coupling elements in the circuit's equation-of-motion matrix) correspond to the admittance inverters $J_{jk}$, and the port dissipation rate $\gamma_{01}$ (respectively, $\gamma_{45}$) corresponds to the admittance inverter $J_{01}$ (respectively, $J_{45}$).



$$2\gamma_0 \mathrm{Im}\Delta_1 = \gamma_{01} = \frac{\Delta\omega}{g_0 g_1} \qquad 2\gamma_0 \mathrm{Im}\Delta_4 = \gamma_{45} = \frac{\Delta\omega}{g_4 g_5}$$
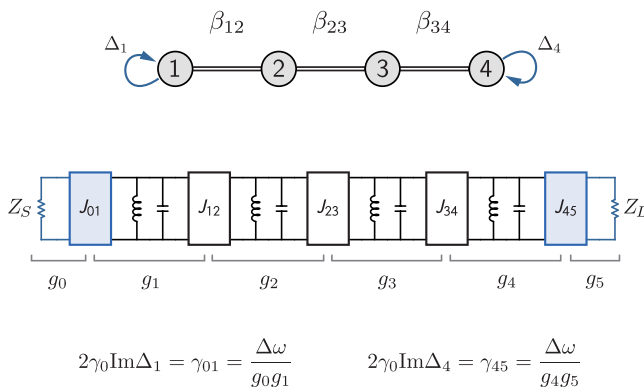
FIG. 13. Correspondence between a graph representation of a parametrically coupled network and a coupled-resonator band-pass filter. The $\beta_{jk}$ are the coupling elements in the coupled-mode matrix representation, $J_{jk}$ are admittance inverters, and $g_i$ are filter prototype coefficients. The port dissipation rates $\gamma$ are embedded in the imaginary part of the self loops on modes 1 and 4.

The coupling rate provided by an admittance inverter $J_{jk}$ disposed between resonant modes $j$ and $k$, in a network design based on prototype with coefficients $\{g_j\}$, is given by [57]

$$c_{jk} = \frac{\Delta\omega}{\sqrt{g_j g_k}}, \tag{58}$$

where $\Delta\omega$ is the bandwidth of the network. The loaded quality factors of the first and last resonators due to their coupling to the environment through $J_{01}$ and $J_{N,N+1}$ are given by [57]

$$\begin{aligned} Q_1 &= \frac{\omega_0}{\Delta\omega} g_0 g_1, \\ Q_N &= \frac{\omega_0}{\Delta\omega} g_N g_{N+1}, \end{aligned} \tag{59}$$

where $\omega_0$ is the network's center frequency.

Comparing Eqs. (58) and (59) to Eqs. (6) and (11), respectively, we arrive at our main result: that a correspondence between the coupled-mode picture and filter synthesis can be made by the relations

$$\gamma_{01} = \frac{\Delta\omega}{g_0 g_1}, \tag{60}$$

$$\gamma_{N,N+1} = \frac{\Delta\omega}{g_N g_{N+1}}, \tag{61}$$

$$\beta_{jk} = \frac{\Delta\omega}{2\gamma_0 \sqrt{g_j g_k}}. \tag{62}$$

Furthermore, comparing to Eqs. (48)–(50) for lumped-element circuits, we have

$$\gamma_{01} = \omega_0 Z_S Z_1 \times J_{01}^2, \tag{63}$$

$$\gamma_{N,N+1} = \omega_0 Z_L Z_N \times J_{N,N+1}^2, \tag{64}$$

$$\beta_{jk} = \frac{\omega_0}{2\gamma_0} \sqrt{Z_j Z_k} \times J_{jk}, \tag{65}$$

where $Z_S$ and $Z_L$ are the source and load impedances, and $Z_j$ is the impedance of mode $j$. Note that, when inverters are connected between modes of different frequencies, the normalized bandwidth $w$ should always be calculated with respect to the reference frequency, so that the absolute bandwidth $\Delta\omega$ is fixed throughout the whole circuit.

Below we demonstrate how we can use the above correspondence to design parametrically coupled circuits with prescribed transfer characteristics.

### B. Synthesis of a parametric frequency converter

In Sec. II C 1 we claimed that a two-mode frequency converter, designed for perfect port match, exactly implements a second-order Butterworth filter. We can now see
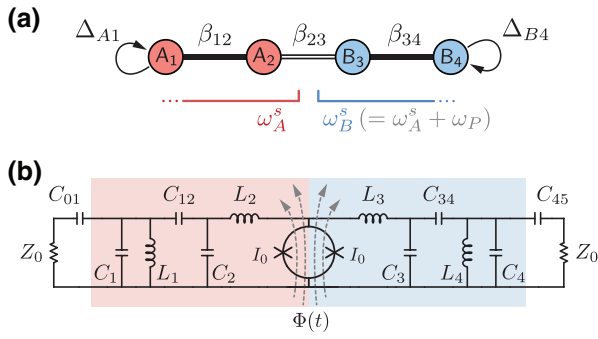
FIG. 14. (a) Coupling graph of a four-mode matched parametric frequency converter, (b) circuit schematic.



FIG. 15. $S$ parameters of a matched parametric converter, calculated using Eq. (8) and the coupling matrix in Eq. (66). The frequency axis is referenced to the signal port.

that indeed, when using the coefficients for the appropriate prototype [28], $g_i = \{1.0, 1.4142, 1.4142, 1.0\}$, in Eqs. (60)–(62) we obtain the same values found in Sec. II C 1, i.e., $\gamma_{01} = \gamma_{23} = \Delta\omega/\sqrt{2}$ and $\beta_{12} = 0.5$.

As a further example, we design a parametric frequency converter with a signal frequency of $\omega_A/2\pi = 5$ GHz, an idler frequency of $\omega_B/2\pi = 7$ GHz, and with a bandwidth of $\Delta\omega/2\pi = 250$ MHz. To facilitate the broadbanding of the usual two-mode converter (Sec. II C 1), we add to the circuit an additional mode at each of the signal and idler frequencies, and design the circuit as a whole to have response characteristics of a four-pole Chebyshev network with 0.01 dB ripple.

The coupled-mode graph for the design is shown in Fig. 14(a). There are two $A$ modes at frequency $\omega_A$ and two $B$ modes at frequency $\omega_B$. Mode $A_1$ is coupled to an external port with rate $\gamma_{01}$ (indicated by the self-loop, with $\gamma_{01} = 2\gamma_0 \text{Im}\{\Delta_{A1}\}$), and mode $B_4$ is coupled to an external port with rate $\gamma_{45}$ (indicated by the self-loop, with $\gamma_{45} = 2\gamma_0 \text{Im}\{\Delta_{B4}\}$). Modes $A_1$ and $A_2$ are at the same frequency and are coupled with a passive element, and similarly for modes $B_3$ and $B_4$. Modes $A_2$ and $B_3$ are coupled by a parametric frequency conversion process with a pump tuned to $\omega_P = \omega_B - \omega_A$.

We can write the equation-of-motion matrix associated with the graph in Fig. 14(a) as

$$\mathbf{M} = \begin{bmatrix} \Delta_{A1} & \beta_{12} & 0 & 0 \\ \beta_{12} & \Delta_{A2} & \beta_{23} & 0 \\ 0 & \beta_{23}^* & \Delta_{B3} & \beta_{34} \\ 0 & 0 & \beta_{34} & \Delta_{B4} \end{bmatrix}. \quad (66)$$

We use design tables [28,57] to find the appropriate prototype coefficients for a four-pole Chebyshev network with the required 0.01 dB ripple,

$$g_i = \{1.0, 0.7128, 1.2003, 1.3212, 0.6476, 1.1007\},$$

and calculate the values of the coupling terms using Eq. (62) to get $\beta_{12} = \beta_{34} = 0.385$ for the passive couplings
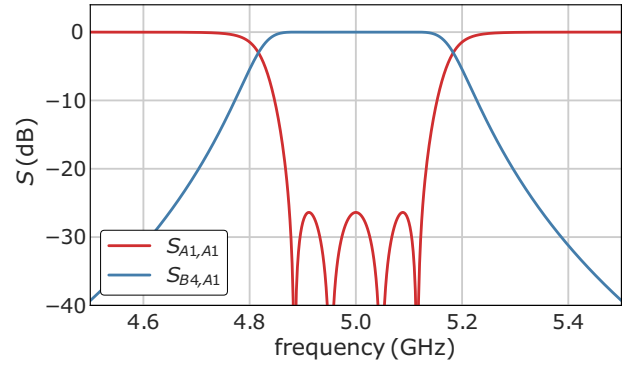
and $|\beta_{23}| = 0.283$ for the parametric coupling. The port coupling rates can be calculated using Eqs. (60) and (61) to obtain $\gamma_{01}/2\pi = \gamma_{45}/2\pi = 351$ MHz.

Figure 15 shows the resulting $S$ parameters, calculated using Eq. (8) for the coupling matrix in Eq. (66) with the parameter values above. The trace labeled $S_{A1,A1}$ is the reflection off of mode $A_1$, and the trace labeled $S_{B4,A1}$ is the transmission through the circuit, equivalent to the conversion gain. Since this is a Chebyshev network, the bandwidth parameter corresponds to the extent of the ripple (0.01 dB in this case) rather than to the 3 dB points [28].

A circuit implementation for a Josephson parametric frequency converter with the above characteristics is shown schematically in Fig. 14(b). The parametric coupler is a dc SQUID with a total critical current of $2I_0 = 2.74$ µA ($L_J = 120$ pH). The inductors $L_2$ and $L_3$ in Fig. 14(b) are both 1.2 nH, resulting in resonator impedances $Z_2 = 44.8$ Ω and $Z_3 = 58.9$ Ω when the SQUID is biased to its operating point. We choose the impedances of the other resonators $Z_1$ and $Z_4$ to equal 35 and 45 Ω, respectively, so that $L_1 = Z_1/\omega_A = 1.11$ nH and $L_4 = Z_4/\omega_B = 1.02$ nH. Remember that we have quite a bit of flexibility in choosing the resonator impedances—these should be chosen in accordance with the fabrication process capabilities, and the values here are merely for demonstration purposes.

With the resonator impedances now set, we use Eqs. (48)–(50) to calculate the values of the admittance inverters. Inverter $J_{23}$ is implemented as the parametric coupler and its value determines the pump amplitude. The remaining inverters are implemented as capacitive $\pi$ sections, Fig. 11(b), and from their values we calculate the capacitances $C_{01} = 212$ fF, $C_{12} = 43$ fF, $C_{34} = 17$ fF, and $C_{45} = 110$ fF. Finally, capacitors $C_1 = 0.675$ pF, $C_2 = 0.667$ pF, $C_3 = 0.369$ pF, and $C_4 = 0.384$ pF are calculated similarly to Sec. IV D.

Figure 16 shows $S$ parameters from circuit simulations of Fig. 14(b) with the component values given above. The solid lines represent $S_{11}$ (red) and $S_{21}$ (blue) from
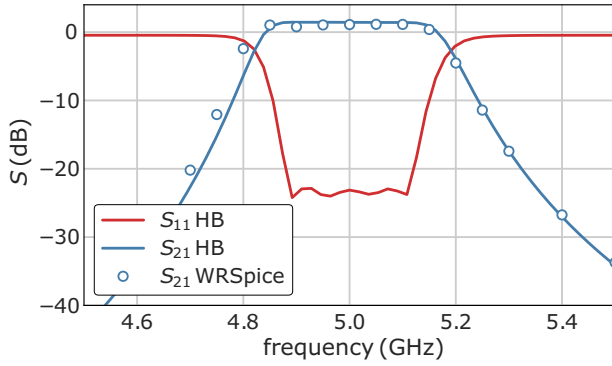
FIG. 16. Simulated $S$ parameters of a matched parametric converter versus frequency referenced to the signal frequency. Solid lines are harmonic-balance simulations in Keysight ADS, circles are data from simulation in WRSpice. In the figure $S_{21} > 0$ dB is a consequence of the Manley-Rowe relations [29], requiring power gain in an up-converting process that has unity photon gain.

harmonic-balance simulation in Keysight ADS, where the dc-SQUID parametric coupler is modeled as a numerically pumped inductance $L = L_J / \cos \pi \phi$ (see Appendix B), with $\phi = \phi_{\mathrm{dc}} + \phi_{\mathrm{ac}} \cos(\omega_P t)$, $\phi_{\mathrm{dc}} = 0.224$, $\phi_{\mathrm{ac}} = 0.18$, and $\omega_P / 2\pi = 2$ GHz. Circles represent $S_{21}$ data from a simulation in WRSpice [63] that includes a full model of the Josephson junctions. In this simulation the SQUID is biased with $\Phi_{\mathrm{dc}} = 0.224\Phi_0$ as above, and pumped at $\omega_P / 2\pi = 2$ GHz with $\Phi_{\mathrm{ac}} = 0.2\Phi_0$.

The simulations are in good mutual agreement, and both are in reasonable agreement with the calculated $S$ parameters in Fig. 15. Notably, both circuit simulations (Fig. 16) show conversion gain of approximately 1.1 dB, consistent with a predicted $G = 10 \log_{10}(\omega_B / \omega_A) = 1.46$ dB based on the Manley-Rowe relations [29,42], whereas $S$ parameters calculated using Eq. (8) (Fig. 15) yield a maximum $G = 0$ dB. The latter result reflects the expected conservation of photon number under ideal frequency conversion.

### C. Broadband parametric circulator

The parametric circulator as described by Ref. [9] consists of three modes connected pairwise via parametric frequency conversion processes. One of the pumps can have a phase of $\pi/2$ with respect to the others, giving rise to circulation. The circuit was already discussed in Sec. II C.

#### 1. Matching strategy

To broadband match the parametric circulator, we adopt the ideas of Anderson [64], which were originally applied to ferrite circulators. We approximate the working circulator as a single effective $LCR$ resonator, whose quality factor depends on parametric coupling strengths $\beta$ in the three-mode "core"; see Fig. 5(a). We then design a network to

match this effective resonated load following Sec. IV C, by finding the values of $\beta$ that satisfy the decrement condition in Eq. (52) for our choice of network prototype.

In general, each port of the three-mode core circuit can be outfitted with a different matching network (having a different prototype, number of sections, or bandwidth); however, here we choose to illustrate the design concepts with a simple, symmetric design, which can be fully worked out analytically. If all ports have equal coupling to the environment $\gamma_A = \gamma_B = \gamma_C$ and all parametric coupling strengths are equal, the circulator circuit has cyclic symmetry, suggesting that the analysis that follows can be done equivalently on either of the bare circulator modes, and that the same matching network parameters (bandwidth and prototype coefficients) can be used on all ports.

The coupling matrix of the bare circulator, Fig. 5, with all coupling strengths set to equal $\beta_c$ (as in Sec. II C 3, we factor out the phase of the coupling and write it out explicitly; therefore, $\beta_c$ is real below) and equal port dissipation rates, is

$$\mathbf{M}_c = \begin{bmatrix} \Delta_{A1} & i\beta_c & \beta_c \\ -i\beta_c & \Delta_{B1} & \beta_c \\ \beta_c & \beta_c & \Delta_{C1} \end{bmatrix}. \quad (67)$$

Using Eq. (12), we can calculate the admittance seen from any of the ports. For example, the admittance seen from port $A$ is

$$\frac{Y_A}{Y_0} = -2i \frac{\Delta_{A1}\Delta_{B1}\Delta_{C1} - \beta_c^2(\Delta_{A1} + \Delta_{B1} + \Delta_{C1})}{\Delta_{B1}\Delta_{C1} - \beta_c^2} - 1, \quad (68)$$

whose real part at the center of the band $\omega = \omega_A$ is

$$\mathrm{Re}\left\{\frac{Y_A}{Y_0}\right\} = \frac{8\beta_c^2}{1 + 4\beta_c^2}. \quad (69)$$

We approximate the slope of the imaginary part of the admittance using the line connecting the points $\mathrm{Im}\{(Y_A(\omega_A \pm \gamma_0/2)/Y_0)\}$, i.e., the average slope over the target frequency band (see Fig. 17). From here, using Eq. (51), we find the quality factor of the effective resonated load presented at the signal port as a function of the coupling strength $\beta_c$:

$$Q = \frac{\omega_A}{\gamma_0} \frac{12\beta_c^3 - 6\beta_c^2 + 2\beta_c + 1}{8\beta_c^2}. \quad (70)$$

If the network that we choose to match the circulator with is symmetric, such that its prototype coefficients satisfy $g_0 g_1 = g_N g_{N+1}$, then Eq. (70), together with Eq. (60) for $\gamma_0$, and the decrement relation Eq. (52), result in $12\beta_c^3 - 14\beta_c^2 + 2\beta_c + 1 = 0$, of which $\beta_c = 0.5$ is a root. If the
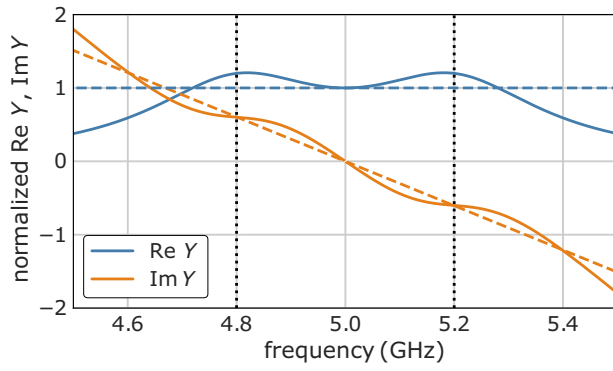
FIG. 17. Real and imaginary parts of the normalized port admittance (solid), along with their approximation (dashed) for the purpose of matching circuit design. Vertical dashed lines indicate detunings of $\pm\gamma_0/2$.



FIG. 18. $S$ parameters of a broadband matched parametric circulator. Here $S_{AA}$ (red) is the reflection from port $A$, and $S_{CA}$ (green) and $S_{BA}$ (blue) are forward and reverse transmissions, respectively. Dashed lines show the forward transmission and reverse isolation of a bare three-mode circulator having the same $\gamma_0$.

network is not symmetric then $\beta_c$ can be found numerically in a similar fashion. The normalized admittance of the bare circulator with $\beta_c = 0.5$ is shown in Fig. 17 (solid lines) along with the resonated load approximation (dashed lines), for $\gamma_0/2\pi = 400$ MHz.

We are now ready to embed the bare circulator in a matching network. We choose a three-pole Chebyshev prototype with 0.01 dB ripple, with coefficients [57] $g_i = \{1.0, 0.6291, 0.9702, 0.6291, 1.0\}$, and build the network by adding two additional, passively coupled modes to each port of the bare circulator. The resulting graph is shown in Fig. 19(a) below, and the corresponding $9 \times 9$ equation-of-motion matrix can be written in the mode basis $\vec{v} = [A_3, B_3, C_3, A_2, B_2, C_2, A_1, B_1, C_1]$ in the block form

$$\mathbf{M} = \begin{bmatrix} \hat{\Delta}_3 & \hat{\beta}_{23} & \hat{0} \\ \hat{\beta}_{23} & \hat{\Delta}_2 & \hat{\beta}_{12} \\ \hat{0} & \hat{\beta}_{12} & \mathbf{M}_c \end{bmatrix}, \qquad (71)$$

where the $3 \times 3$ blocks are $\hat{\Delta}_k = \text{diag}(\Delta_{Ak}, \Delta_{Bk}, \Delta_{Ck})$, $\hat{\beta}_{jk} = \beta_{jk}\mathbb{I}$, $\mathbf{M}_c$ is the bare circulator matrix in Eq. (67), and $\hat{0}$ is a $3 \times 3$ block of zeros. Choosing a bandwidth of 250 MHz and a center frequency of $\omega_A/2\pi = 5$ GHz, and using Eqs. (61) and (62), we obtain $\gamma_0/2\pi = 400$ MHz, $\beta_{12} = \beta_{23} = 0.403$, and $\beta_c = 0.5$ was found above.

Figure 18 shows an $S$-parameter calculation using Eq. (8) with the matrix in Eq. (71). The trace labeled $S_{AA}$ (red) is the reflection from port $A$, $S_{CA}$ (green) is the forward transmission at the direction of the circulation, from port $A$ to port $C$, and $S_{BA}$ (blue) is the reverse transmission from port $A$ to port $B$. We see that over the bandwidth of the device we get flat transmission with low insertion loss in the forward direction, and better than 20 dB reverse isolation. Figure 18 also shows the transmission and reverse isolation (dashed lines) of a bare three-mode circulator
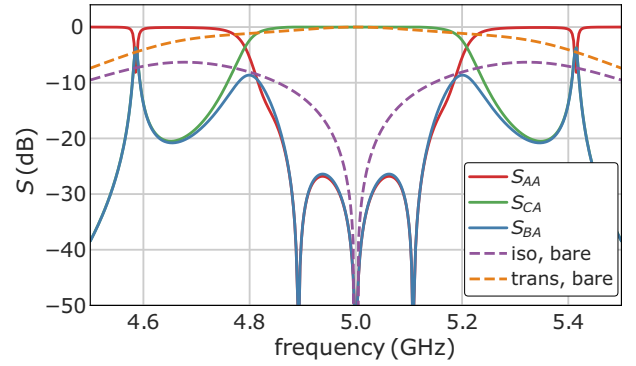
having the same $\gamma_0$, demonstrating the benefit of broadband matching the circulator in improving the bandwidth of usable isolation.

### 2. Circuit implementation

In Sec. II C 3, we mentioned that the minimal construction of a parametric circulator requires only one of the modes to be at a different frequency than the others. For the circuit implementation of the matched circulator, we take advantage of this feature, and set the frequencies of both the $A$ and $C$ modes to 5 GHz, while the $B$ mode frequency is set to 7 GHz. We design with the same prototype as above, and with the same bandwidth of 250 MHz.

The circuit schematic is shown in Fig. 19(b). The parametric couplings between modes $A1$ and $B1$, and between modes $C1$ and $B1$, are implemented here using rf-SQUID couplers [51,52]. The coupling between modes $A1$ and $C1$ is now passive since these modes are resonant, and can be implemented using a capacitive admittance inverter whose value can be calculated from the $\beta_c = 0.5$ we found in the previous section, using Eq. (65):

$$C_{AC} = \frac{J_c}{\omega_A} = \frac{2\gamma_0\beta_c}{\omega_A^2\sqrt{Z_{A1}Z_{C1}}}. \qquad (72)$$

For the circuit in Fig. 19(b), we have $Z_{A1} = Z_{C1} = 6.283$ Ω, giving $C_{AC} = 0.403$ pF. The rest of the elements are calculated in a similar fashion to what we have done in Sec. V B. All component values are listed in Table I.

Figure 19(c) shows the results of a harmonic-balance simulation with the rf SQUIDs modeled as numerically pumped mutuals $M = M_0 + \delta M \cos(\omega_P t)$. Both rf SQUIDs are assumed to be biased such that they provide zero passive mutual coupling, $M_0 = 0$, and both are pumped at $\omega_P/2\pi = 2$ GHz so that the mutual is modulated by $\delta M = 20$ pH, and the phase of the drive to
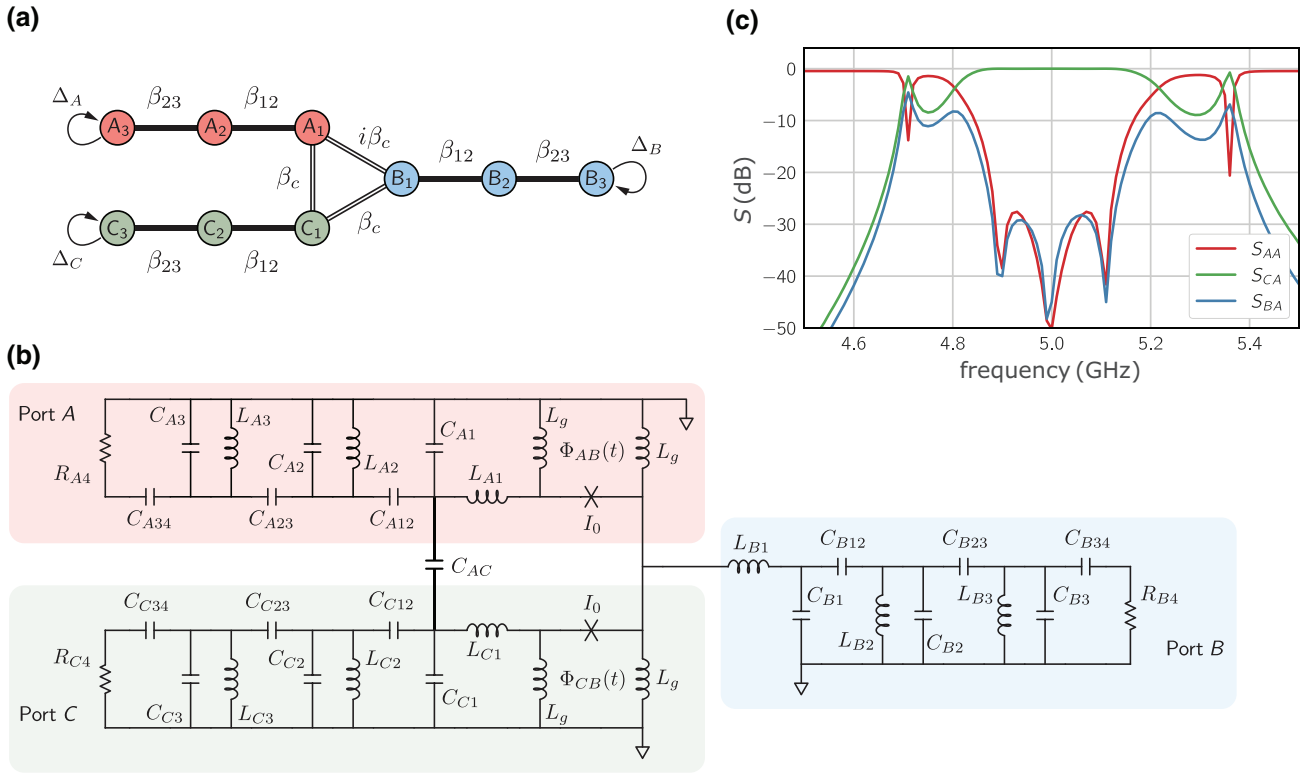
FIG. 19. (a) Coupled-mode graph of a matched parametric circulator. (b) Circuit implementation of a Josephson parametric circulator with ports $A$ and $C$ operating at 5 GHz, and port $B$ operating at 7 GHz. Component values are given in Table I. (c) $S$ parameters from harmonic-balance simulation. Here $S_{AA}$ (red) is the reflection from port $A$, and $S_{CA}$ (green) and $S_{BA}$ (blue) are forward and reverse transmissions, respectively.

the $C - B$ coupler is 87° with respect to that of the $A - B$ coupler. In the simulation, an adjustment of the $C - B$ coupler pump phase away from the ideal 90° is used to compensate for parasitic frequency dependence of the capacitor networks implementing the admittance inverters.

TABLE I. Values of circuit components appearing in Fig. 19(b), and used in the simulation shown in Fig. 19(c).

| Capacitors | Value (pF) | Inductors | Value (nH) |
|---|---|---|---|
| $C_{A1}, C_{C1}$ | 4.515 | $L_{A1}, L_{C1}$ | 0.05 |
| $C_{A2}, C_{C2}$ | 0.845 | $L_{A2}, L_{C2}$ | 0.955 |
| $C_{A3}, C_{C3}$ | 0.777 | $L_{A3}, L_{C3}$ | 0.955 |
| $C_{B1}$ | 2.886 | $L_{B1}$ | 0.100 |
| $C_{B2}$ | 0.655 | $L_{B2}$ | 0.682 |
| $C_{B3}$ | 0.590 | $L_{B3}$ | 0.682 |
| $C_{AC}$ | 0.403 | $L_g$ | 0.150 |
| $C_{A12}, C_{C12}$ | 0.148 | | |
| $C_{A23}, C_{C23}$ | 0.068 | | |
| $C_{A34}, C_{C34}$ | 0.249 | | |
| $C_{B12}$ | 0.068 | | |
| $C_{B23}$ | 0.035 | | |
| $C_{B34}$ | 0.147 | | |

The $S$ parameters from circuit simulations are in reasonable agreement with the calculated $S$ parameters in Fig. 18, which is remarkable considering the vastly different methods and tools used to obtain these results. This agreement gives us confidence in the foundational relations that we established here between the coupling matrix language and that of band-pass network synthesis.

### D. Matched Josephson parametric amplifiers

A matched degenerate Josephson parametric amplifier based on filter design techniques was already demonstrated in Ref. [7]. Roy *et al.* [6] derived a matching circuit for a Josephson parametric amplifier from first principles rather than using techniques from microwave engineering; in Sec. V D 2 we show that their result is equivalent to a two-pole Butterworth matching circuit design.

The Josephson parametric amplifier, like its varactor-based predecessors [42], is a negative-resistance amplifier in which the pumped nonlinear element—typically a SQUID—presents the signal port with a negative effective resistance [49]: this is the admittance of the idler circuit as transformed through the anticonjugating admittance inverter of Eq. (39), as illustrated by Eq. (40). The stray linear shunt inductance of the SQUID, $L_0'$ in Fig. 8(b),

is resonated by adding a shunt capacitance. Therefore, the amplifier can be matched using the techniques of Sec. IV C for matching resonated loads. Observe, however [42,57], that the reflection (voltage) gain off of a negative resistance $-|R_{PA}|$, $\sqrt{G} = (-|R_{PA}| - Z_0)/(-|R_{PA}| + Z_0)$, is equivalent to the inverse of the usual reflection coefficient off of a positive resistance $|R_{PA}|$, $\rho = (|R_{PA}| - Z_0)/(|R_{PA}| + Z_0)$, so that $\sqrt{G} = 1/\rho$. Therefore, when we design the matching circuit, we will design for a finite reflection—an engineered mismatch—that is either flat or has a specified ripple over the band when the network is terminated by $|R_{PA}|$. This is a different requirement than what is used in typical filter and matching networks (where the goal is to approximate $\rho = 0$), so we cannot use the usual network prototypes designed for those situations. Appendix E shows how to calculate suitable prototypes based on Butterworth and Chebyshev response characteristics. Tables of Chebyshev prototypes for matching negative-resistance amplifiers can also be found in Ref. [47].

As already mentioned, physical realizations of immittance inverters carry their own parasitic frequency dependence; this is true as well for the pumped nonlinear element, i.e., $|R_{PA}|$ is some function of frequency; see, for example, Eq. (40). We proceed here to use the value of $|R_{PA}|$ at the center of the band, with the understanding that these methods are best suitable for designs with fractional bandwidths of up to approximately 20%.

### 1. Broadband nondegenerate amplifier

Here we design a nondegenerate parametric amplifier with a bandwidth of 500 MHz, a signal band centered at 5 GHz, an idler band centered at 7 GHz, and using a three-pole Chebyshev prototype designed for 20 dB signal gain and 0.5 dB gain ripple. From Appendix E (Table III) we calculate the prototype coefficients:

$$\{g_0, \ldots, g_4\} = \{1.0, 0.5899, 0.6681, 0.3753, 0.9045\}$$

with $g_0$ corresponding to the amplifier's negative resistance and $g_4$ to the 50 Ω port. Both signal and idler circuits will use the same prototype—this is not necessary, but is convenient.

Figure 20(a) shows the coupled-mode graph for the amplifier, where the conjugated $B^*$ modes are distinguished by their open face shading. Modes $A_1$ and $B_1^*$ are coupled via a parametric coupler pumped at the sum frequency $\omega_P = \omega_A + \omega_B = 12$ GHz. All other couplings between same-frequency modes are passive, and modes $A_3$ and $B_3^*$ are connected to ports.

The $6 \times 6$ equation-of-motion matrix is tridiagonal in the mode basis $\vec{v} = [A_3, A_2, A_1, B_1^*, B_2^*, B_3^*]$, and can be written by inspection using the anticonjugation rules in
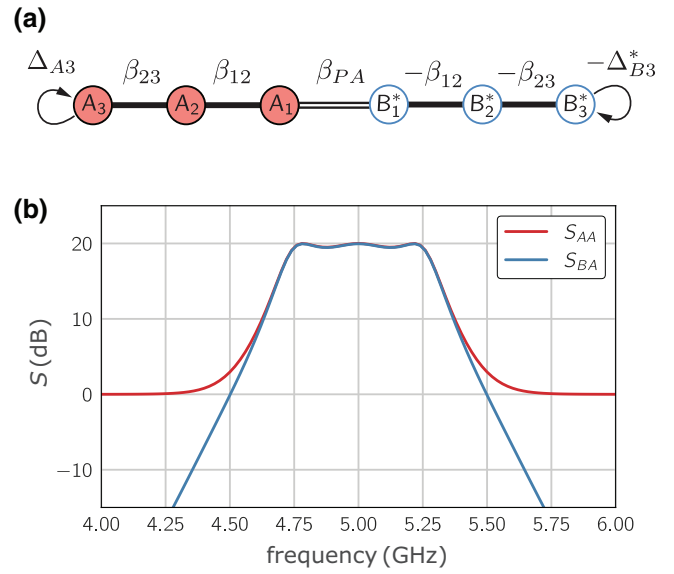
**(a)**



**(b)**



FIG. 20. (a) Coupled-mode graph for a matched nondegenerate parametric amplifier, (b) $S$ parameters for a matched parametric amplifier. Here $S_{AA}$ is the signal reflection gain, and $S_{BA}$ is the signal-idler trans-gain.

Fig. 1 for the $B$ (idler) modes:

$$\mathbf{M}_{PA} = \begin{bmatrix} \Delta_{A3} & \beta_{23} & 0 & 0 & 0 & 0 \\ \beta_{23} & \Delta_{A2} & \beta_{12} & 0 & 0 & 0 \\ 0 & \beta_{12} & \Delta_{A1} & \beta_{PA} & 0 & 0 \\ 0 & 0 & -\beta_{PA}^* & -\Delta_{B1}^* & -\beta_{12} & 0 \\ 0 & 0 & 0 & -\beta_{12} & -\Delta_{B2}^* & -\beta_{23} \\ 0 & 0 & 0 & 0 & -\beta_{23} & -\Delta_{B3}^* \end{bmatrix}.$$

(73)

From the network prototype coefficients $g_i$, we calculate the coupling terms for the passive elements, $\beta_{23} = 0.339$ and $\beta_{12} = 0.270$, using Eq. (62). The parametric coupling term $|\beta_{PA}| = 0.287$ can be found using Eq. (83) in Sec. V D 3. The port coupling rates are $\gamma_0/2\pi = 1.476$ GHz.

Figure 20(b) shows $S$ parameters calculated with Eq. (8) and the matrix in Eq. (73) with the parameters above. In the figure, $S_{AA}$ is the signal reflection gain from port $A_3$ and $S_{BA}$ is the idler trans-gain at port $B_3^*$.

Circuit implementations will vary based on the coupler architecture (see Appendix C), but after fixing the impedances of the resonators embedding the coupler, all other circuit components can be readily calculated using the network prototypes and Eqs. (49) and (50), as was demonstrated in detail in the preceding sections.

### 2. Analysis of Roy et al.

Roy *et al.* [6] were the first to describe a Josephson parametric amplifier with a synthesized impedance matching network. A schematic of the circuit is shown in
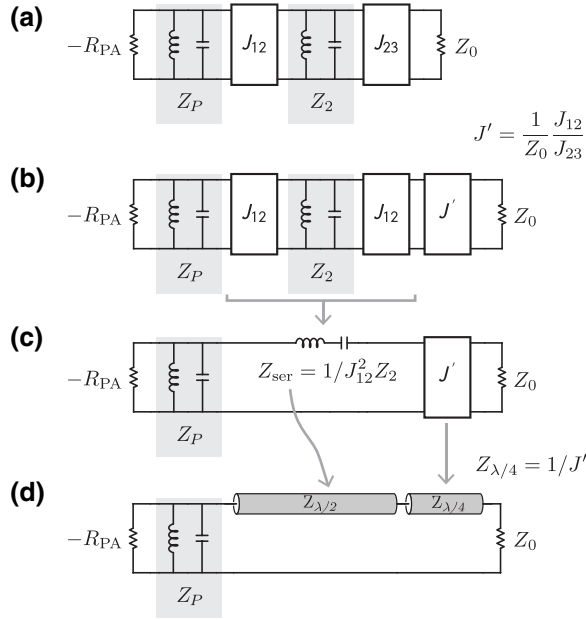
FIG. 21. Transformation used to go from shunt coupled resonators to ladder configuration with series auxiliary mode (a, b, c), and finally to the transmission-line topology of Ref. [6] (d). The pumped junction is represented by a negative resistance $-R_{\mathrm{PA}}$.

Fig. 21(d), where the pumped capacitively shunted SQUID is represented by the negative resistance $-R_{\mathrm{PA}}$ in parallel with the resonator $Z_p$. Broadband impedance matching of the device is accomplished via a series combination of two transmission line resonators, as shown in the figure. The simplicity of this particular implementation makes it amenable to fabrication with modest resources, while producing relatively wide bandwidth. The basic design has been recently reproduced in Refs. [65,66] albeit with small modifications. Despite its approachability, the design parameters were derived using a physics approach, and modifications to the gain, bandwidth and center frequency are less straightforward to produce [65].

Here, we show that the design of Ref. [6] can be derived from a synthesized two-pole network with Butterworth characteristics. The plan is to start with a two-pole matching network prototype suitable for negative resistance amplifiers. One of the poles is the resonated SQUID, the other pole is what Ref. [6] calls the "auxiliary resonator." We first show how to obtain design parameters for a ladder circuit as shown in Fig. 21(c), and then transform it to the circuit topology of Ref. [6] [Fig. 21(d)].

For a given center frequency $\omega_0$ and bandwidth $\Delta\omega$, the design is fully constrained by the inductance $L_p$ of the Josephson circuit, in this case a dc SQUID, at the operating flux bias point. This is resonated out with a shunt capacitor $C_p$, to match a target frequency $\omega_0$. The design in Ref. [6] had $\omega_0/2\pi = 6$ GHz and $w = \Delta\omega/\omega_0 \approx 0.1$,

and the capacitance shunting the SQUID was $C_p = 3.4$ pF. From this, $Z_p = 1/\omega_0 C_p = 7.8\,\Omega$.

We use a two-pole max-flat (Butterworth) prototype with 20 dB gain, calculated according to Appendix E (Table II):

$$\{g_0,\ldots,g_3\} = \{1.0,\ 0.408,\ 0.234,\ 1.106\} \qquad (74)$$

with $g_0$ the pumped junction and $g_3$ the 50 $\Omega$ load. To obtain the desired ladder topology of Fig. 21(c), it is natural to use the method of Sec. IV A. From Eq. (44) we have

$$Y_p = g_1 \frac{\omega_0}{\Delta\omega} Y_{\mathrm{ref}}, \qquad (75)$$

where $Y_{\mathrm{ref}}$ is the reference admittance. Usually, we have $Y_{\mathrm{ref}} = Y_0 = (50\ \Omega)^{-1}$; however, here, since $Y_p = 1/Z_p$ is constrained, we use this equation instead to find the appropriate reference impedance for the network,

$$Z_{\mathrm{ref}} = \frac{1}{Y_{\mathrm{ref}}} = g_1 \frac{\omega_0}{\Delta\omega} Z_p = 31.8\ \Omega. \qquad (76)$$

Using $Z_{\mathrm{ref}}$ above in Eq. (45), we can now find the impedance of the series "auxiliary" resonator:

$$Z_{\mathrm{ser}} = g_2 \frac{\omega_0}{\Delta\omega} Z_{\mathrm{ref}} = 74.4\ \Omega. \qquad (77)$$

Finally, the load impedance, Eq. (46), is denormalized to $Z_L = Z_{\mathrm{ref}}/g_3 = 28.8\ \Omega$. To transform $Z_L$ to the $Z_0 = 50\ \Omega$ environment, we insert an admittance inverter, $J'$ in Fig. 21(c), whose value is

$$J' = 1/\sqrt{Z_L Z_0} = 0.0264\ \Omega^{-1}. \qquad (78)$$

For completeness, before proceeding to the implementation of the circuit shown in Fig. 21(d), we show how the same circuit parameters can be derived using an approach based on the method in Sec. IV B. We start from the same prototype coefficients and the constrained value of $Z_p$ above, and construct the circuit of Fig. 21(a), where the inverter values can be calculated in the usual way [Eqs. (48)–(50)] and we assume some arbitrary value for $Z_2$. Next, we factor $J_{23}$ into a series combination of $J_{12}$ and $J' = (1/Z_0)(J_{12}/J_{23})$, as shown in Fig. 21(b), and transform the shunt resonator $Z_2$ and the adjacent inverters into a series resonator, $Z_{\mathrm{ser}} = 1/J_{12}^2 Z_2 = g_1 g_2 Z_p/w^2$, to arrive again at Fig. 21(c). The values of $Z_{\mathrm{ser}}$ and $J'$ found here are identical to those found above using the direct ladder synthesis.

Proceeding with the circuit implementation of Ref. [6], the series resonator is implemented as a half-wave transmission line resonator with impedance $Z_{\lambda/2}$, and the inverter $J'$ is implemented as a quarter-wave transmission line with impedance $Z_{\lambda/4}$. The two transmission lines are in series with each other, as shown in Fig. 21(d).

The impedance $Z$ seen looking through the series resonator $Z_{\text{ser}}$ towards a load $Z_L = 1/J'^2 Z_0$ [Fig. 21(c)] near the resonance frequency can be approximated as (writing $\omega = \omega_0 + \delta\omega$)

$$Z = Z_L + 2jZ_{\text{ser}}\frac{\delta\omega}{\omega_0}. \tag{79}$$

Likewise, the impedance $Z'$ seen through a half-wave transmission line with $Z_{\lambda/2}$ in series with a quarter-wave transmission line with $Z_{\lambda/4}$ [Fig. 21(d)] near the resonance frequency $\omega_0$ is

$$Z' \simeq \frac{Z_{\lambda/r}^2}{Z_0} + j\frac{\pi}{2}\frac{\delta\omega}{\omega_0}\left[Z_{\lambda/4}\left(1 - \frac{Z_{\lambda/4}^2}{Z_0^2}\right)\right.$$
$$\left. + 2Z_{\lambda/2}\left(1 - \frac{Z_{\lambda/4}^4}{Z_0^2 Z_{\lambda/2}^2}\right)\right]; \tag{80}$$

this is the basis for Eq. (S40) of Ref. [6] and Eq. (2) of Ref. [66].

Equating Eqs. (79) and (80), we get the following quadratic equation for $Z_{\lambda/2}$ that we can solve to get the impedance value:

$$Z_{\lambda/2}^2 - Z_{\lambda/2}\left[\frac{2}{\pi}Z_{\text{ser}} - \frac{1}{2}Z_{\lambda/4}\left(1 - \frac{Z_{\lambda/4}^2}{Z_0^2}\right)\right] - \frac{Z_{\lambda/4}^4}{Z_0^2} = 0 \tag{81}$$

with $Z_{\lambda/4} = 1/J'$ [Eq. (78)] and $Z_{\text{ser}}$ found in Eq. (77).

Using the numerical values in Eqs. (77) and (78), we finally get $Z_{\lambda/2} = 54.55\,\Omega$ and $Z_{\lambda/4} = 37.93\,\Omega$. This agrees with the values of $Z_{\lambda/2} \approx 58\,\Omega$ and $Z_{\lambda/4} \approx 40\,\Omega$ reported in Ref. [6].

Figure 22 shows harmonic-balance simulations using a symbolic nonlinear device model in Keysight ADS for the pumped SQUID. All simulation curves use the same
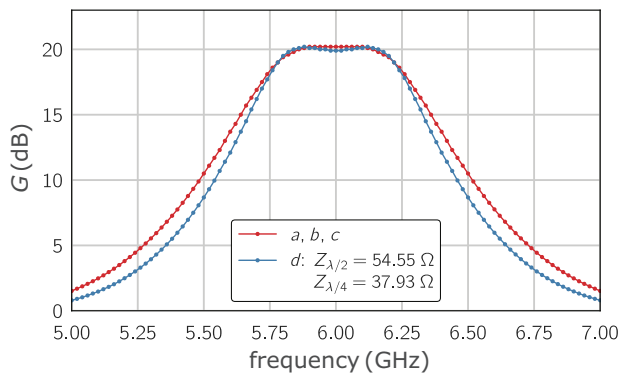


FIG. 22. Keysight ADS harmonic-balance simulations of the circuits in Figs. 21(a)–21(c), and the transmission line implementations, Fig. 21(d), with the parameters indicated in the legend.

flux bias $\Phi_{\text{dc}} = 0.3075\,\Phi_0$ (chosen to get the shunted SQUID resonance frequency to 6 GHz), and pump amplitude $\Phi_{\text{ac}} = 0.111\,\Phi_0$. The curve labeled a, b, c (red) corresponds to the schematics in Figs. 21(a)–21(c), where the inverters are implemented as ideal $Y$ matrices. These circuits produce identical results showing that the transformations in Figs. 21(a)–21(c) are equivalent. The blue trace (d) represents a transmission line resonator implementation as in Ref. [6] corresponding to the schematic in Fig. 21(d), with the transmission line impedances as obtained in this section. The two traces should ideally be equivalent; however, it is not surprising that trace d shows slightly narrower response than the transformations in a, b, c, since it is using approximations that become worse with detuning away from $\omega_0$. The synthesized parameters and simulated response agree with what was reported in Ref. [6], showing that their matched broadband parametric amplifier design can be understood in terms of simple network synthesis methods known from microwave engineering.

### 3. Calculating the parametric amplifier pump amplitude

In Sec. III C we saw that sum-frequency parametric coupling (amplification process) presents the input port with an effective negative resistance, resulting in gain. This negative resistance, as we have seen in Eqs. (38)–(40) and Fig. 8, depends on the pump amplitude. Earlier in this section, we designed matching networks for parametric amplifiers, assuming that the pump amplitude (or, alternatively, the parametric coupling strength $\beta_p$) has been set correctly so that the negative impedance $-|R_{\text{PA}}|$ presented to the matching network satisfies the so-called decrement condition in Eq. (52):

$$Q = |R_{\text{PA}}|/Z_1 = g_0 g_1 / w \tag{82}$$

with $g_0$ and $g_1$ the prototype coefficients, $w$ the fractional bandwidth, and $Z_1$ the impedance of the resonance embedding the modulated inductor.

In the coupled-mode equation-of-motion matrix picture, the pump amplitude is expressed by the dimensionless parametric coupling strength $\beta_p$. We can calculate it as the normalized dissipation rate of resonator $Z_1$ due to the effective resistance $|R_{\text{PA}}|$:

$$\beta_p = \frac{\omega_0}{2\gamma_0}\frac{Z_1}{|R_{\text{PA}}|} = \frac{1}{2}\frac{g_N g_{N+1}}{g_0 g_1}. \tag{83}$$

Here we have used $\gamma_0 = \Delta\omega/g_N g_{N+1}$, Eq. (61), and the decrement relation, Eq. (82).

As a simple check, for the two-mode parametric amplifier of Fig. 2(c) with 20 dB gain, $N = 1$, and, using $g_0 = 1.0$ and $g_2 = 0.9045$ calculated according to Appendix E, it follows from Eq. (83) that $\beta_p = g_2/2g_0 = 0.452$, which recovers the result of Eq. (22).

In a circuit implementation, the pump amplitude is expressed via the parameter $\alpha$, defined in Figs. 8(b) and 9(b). Using the shunt representation in these figures, we can calculate $\alpha$ for a given prototype, signal power gain $G$, and fractional bandwidth $w$ as

$$\alpha = \frac{\sqrt{G} - 1}{\sqrt{G} + 1}\left(\frac{w}{g_1}\right)^2 \times \begin{cases} g_{N+1}^2, & N \text{ even}, \\ g_{N+1}^{-2}, & N \text{ odd}, \end{cases} \qquad (84)$$

as shown in Appendix C.

Equations (83) and (84) are useful in circuit design and simulation. Equation (84) in particular should be used to ensure that the chosen physical implementation of the parametric coupler can deliver the required modulation strength. Knowledge of this quantity can also inform the design of the experimental setup, with respect to, e.g., choice of pump generator, attenuation in the microwave cable delivering the pump, or on-chip coupling architecture. It can also serve as a starting point for experimentally finding the optimal pump power during the amplifier bringup and calibration procedure.

### E. Design flow

As a summary, we outline a general design flow that we have found useful in prototyping and simulating parametrically coupled networks.

1. *Draw the network graph.* For a given required functionality, we find it useful to first sketch the coupling graph (Sec. II B). Doing so we can readily identify the required coupling processes, plan the mode basis, and assign mode frequencies and ports.

2. *Calculate network prototype coefficients.* Based on the desired response characteristics and the topology of the circuit, find the appropriate prototype coefficients $\{g_i\}$, either from tables when appropriate [28,57], or by direct calculation as outlined in Appendix E.

3. *Assign coupling rates.* Given a bandwidth requirement for the circuit, calculate the port dissipation rates $\gamma_k$ using the prototype coefficients and Eqs. (60) and (61). Calculate the normalization rate $\gamma_0$ from Eq. (10), and the coupling terms $\beta_{jk}$ from Eq. (62). For networks involving parametric amplification, use Eq. (83) to calculate $\beta_{PA}$ that corresponds to the sum-frequency pump, as was done in Sec. V D.

4. *Write down the equation-of-motion matrix.* From the network graph, write down the equation-of-motion matrix using the rules in Fig. 1. This step, and indeed steps 2 and 3 as well, are amenable to automation.

5. *Calculate the S parameters.* The $S$ parameters of the design can now be calculated from the equation-of-motion matrix using Eq. (8) to verify the desired behavior of the circuit. It is easy at this step to explore, for example, the effects of different pump phases and amplitudes, or different network prototype coefficients.

6. *Determine parametric coupler implementation.* The configuration of the parametric coupler will constrain the rest of the circuit. In a Josephson junction circuit, we have several options for the coupler, including a shunt-connected dc SQUID (Sec. V B), a rf-SQUID coupler (Sec. V C), or a balanced bridge [39,67], each with their own advantages and ability to incorporate advanced nonlinear devices such as the SNAIL [8] or SQUID arrays [7]. With the implementation fixed, construct resonators to embed the coupler, e.g., by shunting the Josephson element with capacitors to achieve the specified resonance frequency. The impedances of the resonators embedding the coupler will be important parameters in the following steps. Use Eq. (84) or (C5) to ensure that the required modulation strength is consistent with the coupler design.

7. *Determine resonator implementation.* With the resonators embedding the parametric coupler determined in step 6, next choose the implementation (e.g., lumped element, quarter wave, cavity) and impedances of the remaining resonators in the circuit based on the available technology.

8. *Calculate immittance inverters.* With all resonator impedances now known, use Eqs. (48)–(50) to calculate the values of the admittance $J$ inverters. If the resonators are not lumped, or the implementation calls for $K$ inverters instead, refer to Ref. [57] for alternative expressions for inverter values.

9. *Determine inverter implementation.* For $J$ inverters in a lumped-element circuit, choose either a capacitive or inductive circuit (Fig. 11) for each of the inverters, and calculate the component values. Capacitive implementations are favorable in Josephson circuits as they do not introduce additional superconducting loops. Inductive implementations can be advantageous in circuits that require transition between single-ended and balanced sections [67]. Other implementations are more appropriate for $K$ inverters or for distributed components; these can be found in Refs. [28,48,57].

10. *Calculate component values.* Calculate resonator inductance and capacitance values based on the resonator impedance and frequency, and absorb the negative reactances of the adjacent inverters, as demonstrated in Sec. IV D. It is important to check at this point that all component values are realizable in the given technology; iterate through steps 7–9 to fix any issues, as we have flexibility to adjust the resonator impedances.

11. *Perform circuit simulations.* With all component values now known, simulate the circuit in a tool such as Keysight ADS, AWR Microwave Office, or WRSpice using harmonic-balance or transient analyses. The parametric couplers can be approximated as a numerically modulated inductance or mutual inductance, varying at the pump frequency. This step is important as it will reveal any issues stemming from, e.g., the fact that the inverters are not ideal and their reactances are frequency dependent. Most tools allow for manual trimming of component values in real time, and this functionality can be used to manually compensate for nonidealities in components. The designer should also explore here the effects of component variations and parasitics on the performance of the device.

At the completion of the above steps, the design should be ready for layout and manufacture. As noted, many of these steps can be automated based on the rules and equations given in this tutorial, allowing the designer to focus their creative effort on steps 1, 6, and the physical design.

## VI. CONCLUSION AND OUTLOOK

The design of parametrically coupled networks and that of microwave filters both boil down to engineering the mutual coupling rates between resonant modes, and between these modes and the environment. These disciplines, however, approach this problem with seemingly different language, tools, and methods. In this tutorial we have shown that, in fact, a common language can be used to describe both electrical filter networks and parametric networks, regardless of their physical implementation.

We have shown that, given prescribed response characteristics for a 1D-connected system of $N$ modes, which can be fully described by $N + 2$ prototype coefficients, the coupling rates in the system can be calculated from these coefficients to realize the desired response. The correspondence we established between the $\beta$ (coupling efficiency) and $\gamma$ (dissipation rate) of the coupled-mode language, to the admittance (impedance) inverters $J$ ($K$) of the filter synthesis language, offers agility in designing systems that may contain a mix of both passive and parametric couplings. Techniques developed for matching more complicated electrical systems, like ferrite circulators and amplifiers, as well as techniques for designing with internally lossy components, can now be readily used in the context of parametrically coupled devices. The principles outlined here also open the door for microwave engineers and filter designers to have significant impact on key technologies, components, and subsystems in the quantum computer stack.

We presented a range of example designs based on simple filter networks; however, more sophisticated multiply connected structures have been researched, both in the microwave filter arena [54,56] and in Josephson parametric amplifiers [68]. By bridging the gap between these disciplines we hope to spur further research that utilizes advanced filter synthesis methods to produce new and performant parametric amplifiers, transduction networks [61], and nonreciprocal device designs. Further research is also needed to expand on the methods outlined here to include systematic analysis and optimization of quantum noise performance of these networks.

## APPENDIX A: $Z$, $Y$, AND $ABCD$ MATRIX REPRESENTATIONS FOR MODULATED INDUCTORS

In Sec. III we wrote the **Z** matrices for parametrically pumped circuit elements. Here we show how to transform those to $ABCD$ (**T**) matrices and factor the component into passive and purely parametric parts, as we have done in Figs. 8 and 9.

### 1. Equivalent series inverter circuits

The $Z$-matrix form is especially useful in helping to identify a convenient circuit representation. This becomes clear if we convert an arbitrary $Z$ matrix to a transmission ($T$ or $ABCD$) matrix [28]. One can show that the resulting transformation can be factored into three separate matrices,

$$\mathbf{T}(\mathbf{Z}) = \begin{bmatrix} 1 & z_{11} \\ 0 & 1 \end{bmatrix} \begin{bmatrix} 0 & -z_{12} \\ z_{21}^{-1} & 0 \end{bmatrix} \begin{bmatrix} 1 & z_{22} \\ 0 & 1 \end{bmatrix}. \quad (A1)$$

From this form, we see that diagonal elements of the $Z$ matrix represent series impedances, while off-diagonal elements correspond to an inverterlike object sandwiched between these impedances (Fig. 23).

If we substitute into Eq. (A1) the $Z$ matrices we derived for the modulated inductor, Eq. (31) for parametric frequency conversion, and Eq. (37) for parametric amplification, we have the transmission matrix equivalents

$$\mathbf{T}_{L,\mathrm{FC}}^{\mathrm{ser}} = \begin{bmatrix} 1 & j\omega_1 L_0 \\ 0 & 1 \end{bmatrix} \begin{bmatrix} 0 & -jK_1^* \\ -j/K_2 & 0 \end{bmatrix} \begin{bmatrix} 1 & j\omega_2 L_0 \\ 0 & 1 \end{bmatrix}$$
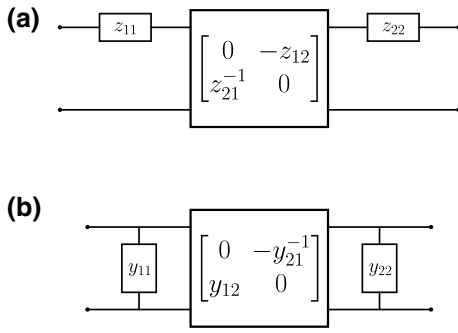$$(A2)$$

FIG. 23. Equivalent two-port circuit networks for an arbitrary (a) $Z$ matrix and (b) $Y$ matrix. The center element is represented by the equivalent inverterlike transmission matrix.

and

$$\mathbf{T}_{L,\mathrm{PA}}^{\mathrm{ser}} = \begin{bmatrix} 1 & j\omega_1 L_0 \\ 0 & 1 \end{bmatrix} \begin{bmatrix} 0 & -jK_1 \\ j/K_2^* & 0 \end{bmatrix} \begin{bmatrix} 1 & -j\omega_2 L_0 \\ 0 & 1 \end{bmatrix}, \tag{A3}$$

where we have defined a complex inverter constant

$$K_\ell \equiv \omega_\ell \frac{\delta L}{2}. \tag{A4}$$

From both of these expressions, we see that the time-invariant part of the inductance, $L_0$, looks like a series inductor, with its impedance reckoned at both the signal ($\omega_1$) and idler frequencies ($\pm\omega_2$). Meanwhile, the inverter's role is to convert current at the signal (idler) frequencies to voltage at the idler (signal) frequencies. The strength of this conversion process is determined by the pump amplitude $|\delta L|$. In Fig. 8(b), we denote this as the *series representation* for the parametrically modulated inductor.

### 2. Equivalent shunt inverter circuits

In building a frequency converter or amplifier circuit, $L_0$ should be regarded as part of the core resonator and corresponding matching sections, which we term the *signal* and *idler matching networks*, each evaluated at their respective frequencies. In the series representation, $L_0$ is used to build the last series $LC$ section in a multipole matching network, up to the inverter. However, it is often the case that parallel-$LC$ sections are easier to implement in a given technology [28,48]. To convert to a *parallel representation*, one can write down a transmission matrix factorization, similar to Eq. (A1), but for the admittance matrix $\mathbf{Y} = \mathbf{Z}^{-1}$:

$$\mathbf{T}(\mathbf{Y}) = \begin{bmatrix} 1 & 0 \\ y_{11} & 1 \end{bmatrix} \begin{bmatrix} 0 & -y_{21}^{-1} \\ y_{12} & 0 \end{bmatrix} \begin{bmatrix} 1 & 0 \\ y_{22} & 1 \end{bmatrix}. \tag{A5}$$

Applying Eq. (A5) with the inverted $Z$ matrices from Sec. III yields an equivalent *shunt representation* [see Fig. 8(b)]

$$\mathbf{T}_{L,\mathrm{FC}}^{\mathrm{shunt}} = \begin{bmatrix} 1 & 0 \\ (j\omega_1 L_0')^{-1} & 1 \end{bmatrix} \begin{bmatrix} 0 & j/J_1' \\ jJ_2'^* & 0 \end{bmatrix} \begin{bmatrix} 1 & 0 \\ (j\omega_2 L_0')^{-1} & 1 \end{bmatrix} \tag{A6}$$

and

$$\mathbf{T}_{L,\mathrm{PA}}^{\mathrm{shunt}} = \begin{bmatrix} 1 & 0 \\ (j\omega_1 L_0')^{-1} & 1 \end{bmatrix} \begin{bmatrix} 0 & j/J_1'^* \\ -jJ_2' & 0 \end{bmatrix}$$
$$\times \begin{bmatrix} 1 & 0 \\ (-j\omega_2 L_0')^{-1} & 1 \end{bmatrix}, \tag{A7}$$

where we have defined an effective shunt inductance

$$L_0' \equiv L_0 \left( 1 - \frac{|\delta L|^2}{4L_0^2} \right) \tag{A8}$$

and inverter constant

$$K_\ell' = J_\ell'^{-1} \equiv \omega_\ell L_0 \left( \frac{2L_0}{\delta L} - \frac{\delta L^*}{2L_0} \right). \tag{A9}$$

The key results of this appendix are summarized, in compact form, in Fig. 8(b). Similar arguments can be used to derive the relations summarized in Fig. 9(b) for the modulated mutual inductance.

## APPENDIX B: JOSEPHSON JUNCTIONS AND SQUIDS AS MODULATED INDUCTORS

The role of the parametric coupler element in Sec. III is played by a modulated inductor, which in Josephson parametric devices can be performed by any of a variety of single and multijunction devices [7,8,39,51]. Here we give a primer on two very simple choices, a single Josephson junction and the dc SQUID.

### 1. Single Josephson junction

The Josephson equations [69,70] yield a simple expression for the inductance of a single junction as a function of bias current $I$,

$$L_J(I) = \frac{\Phi_0}{2\pi I_0} \frac{1}{\sqrt{1 - I^2/I_0^2}}, \tag{B1}$$

where $\Phi_0 \approx 2.068 \ \mu\mathrm{A\,nH}$ is the single flux quantum and $I_0$ is the junction critical current. This is a nonlinear function of the bias current and, if expanded around $I = 0$, in the small current limit, this can be approximated as

$$L_J(I) \simeq L_{J0} \left( 1 + \frac{1}{2} \frac{I^2}{I_0^2} \right), \tag{B2}$$

where we define the Josephson inductance, $L_{J0} \equiv \Phi_0/2\pi I_0$. Modulation of the inductance is achieved

by injecting a pump current, $I_P(t) = |I_P| \cos(\omega_P t + \phi_P)$, yielding a time-dependent inductance

$$L_J^{4\text{w}}(t) \simeq L_{J0}\left[1 + \frac{1}{2}\frac{|I_P|^2}{I_0^2}[1 + \cos(2\omega_P t + 2\phi_P)]\right]$$

$$\simeq L'_{J0} + \delta L \cos(2\omega_P t + 2\phi_P) \qquad (\text{B3})$$

with an effective base inductance

$$L'_{J0} \equiv L_{J0}\left(1 + \frac{1}{2}\frac{|I_P|^2}{I_0^2}\right) \qquad (\text{B4})$$

and inductance modulation amplitude

$$\delta L \equiv \frac{L_{J0}}{2}\frac{|I_P|^2}{I_0^2}. \qquad (\text{B5})$$

#### a. Four-wave mixing

Equation (B3) differs slightly from the expression in Eq. (28) having a modulation frequency $2\omega_P$ instead of $\omega_P$. In this configuration, where we are using a quadratic nonlinearity in the current, the inductance modulation is doubled in frequency. In other words, the nonlinear element is modulated by a subharmonic drive. Since the purpose of this element is to achieve mixing between a signal and idler, we require only that the element modulate at the difference frequency between the two. Therefore, for frequency conversion, we have $2\omega_P = |\omega_1 - \omega_2|$ (connecting $\omega_1$ and $\omega_2$), and for amplification, we have $2\omega_P = \omega_1 + \omega_2$ (connecting $\omega_1$ and $-\omega_2$). This approach is often termed *four-wave mixing*, but can be interpreted as a consequence of using a quadratic nonlinearity to achieve the required mixing product frequencies for parametric coupling.

#### b. Three-wave mixing

Alternatively, one can choose to add a dc bias to the pump current, $I_P(t) = I_{\text{dc}} + |I_P| \cos(\omega_P t + \phi_P)$, in which case the lowest order expansion for the inductance is

$$L_J^{3\text{w}}(t) \simeq L'_{J0} + \delta L \cos(\omega_P t + \phi_P) \qquad (\text{B6})$$

with

$$L'_{J0} \equiv \frac{L_{J0}}{\sqrt{1 - I_{\text{dc}}^2/I_0^2}} \qquad (\text{B7})$$

and

$$\delta L \equiv L_{J0}\frac{I_{\text{dc}}}{I_0}\frac{1}{(1 - I_{\text{dc}}^2/I_0^2)^{3/2}}|I_P|. \qquad (\text{B8})$$

Equation (B6) corresponds to "direct" modulation of the inductance at $\omega_P$ as in Eq. (28), a consequence of the dominant linear dependence of $\delta L$ on current when expanded around a bias current.

While the current nonlinearity above is convenient to use, it requires some care in handling the large pump tone required to modulate the inductance, which can be close to the signal frequency in the case of four-wave mixing, necessitating additional components in the signal path to cancel or filter it out. In practice, these extra components can impact the overall noise performance and complicate operation and bringup.

#### 2. dc SQUID

As an alternative to using the current nonlinearity, one can utilize a loop topology that interferes two supercurrent paths. The result is an effective Josephson inductance that can be tuned by the magnetic flux threading the loop. There are several variants of these SQUID configurations, but in this work, for simplicity, we utilize an ideal dc SQUID. This is comprised of two Josephson junctions in parallel, with no stray inductance and a means to modulate its magnetic flux threading the loop [70]. In the limit where stray inductance is negligible, the inductance has a simple form,

$$L_{\text{SQ}}(I, \Phi) = \frac{L_{J0}(I)}{2|\cos(\pi\Phi_A/\Phi_0)|}, \qquad (\text{B9})$$

where $\Phi_A$ is the magnetic flux induced by an adjacent flux line, and can include both dc and ac components. Here $L_{J0}(I)$ is the single junction current-dependent inductance; see Eq. (B1).

Equation (B9) is a nonlinear, periodic function in the applied flux. As with the Josephson current nonlinearity, one can likewise choose to bias such that the dominant first-order expansion term in flux is either quadratic (four-wave) ($\Phi_{\text{dc}} = 0$) or linear (three-wave) [$|\Phi_{\text{dc}}| \neq 0$ modulo $(n + 1/2)\Phi_0$ for integer $n$]. Just as we did for the current-pumped junction, we can likewise expand the inductance for a given flux pump modulation, $\Phi_A(t) = \Phi_{\text{dc}} + \Phi_P \cos(\omega_P t + \phi_P)$. One can then generate both four-wave [Eq. (B3)] and three-wave [Eq. (B6)] inductance modulation forms as we did above [49].

### APPENDIX C: USING THE *J*- and *K*-INVERTER MODELS OF PARAMETRIC COUPLING IN AMPLIFIER DESIGN

In Figs. 8 and 9, we presented equivalent models for the parametrically modulated inductor and mutual as impedance ($K$) or admittance ($J$) inverters. Here we show how to use these "parametric inverter" models as aids in the synthesis of wideband amplifier circuits, as well as in the systematic calculation of the full two-port response of these circuits. In addition, we show how these inverter models can be used to set the parametric modulation strength, or pump amplitude, based on the bandwidth and response characteristics in a multipole matched amplifier.

As noted in Sec. III C, the immittance inverter models reduce to the "pumpistor model" [49] for reflection JPAs;
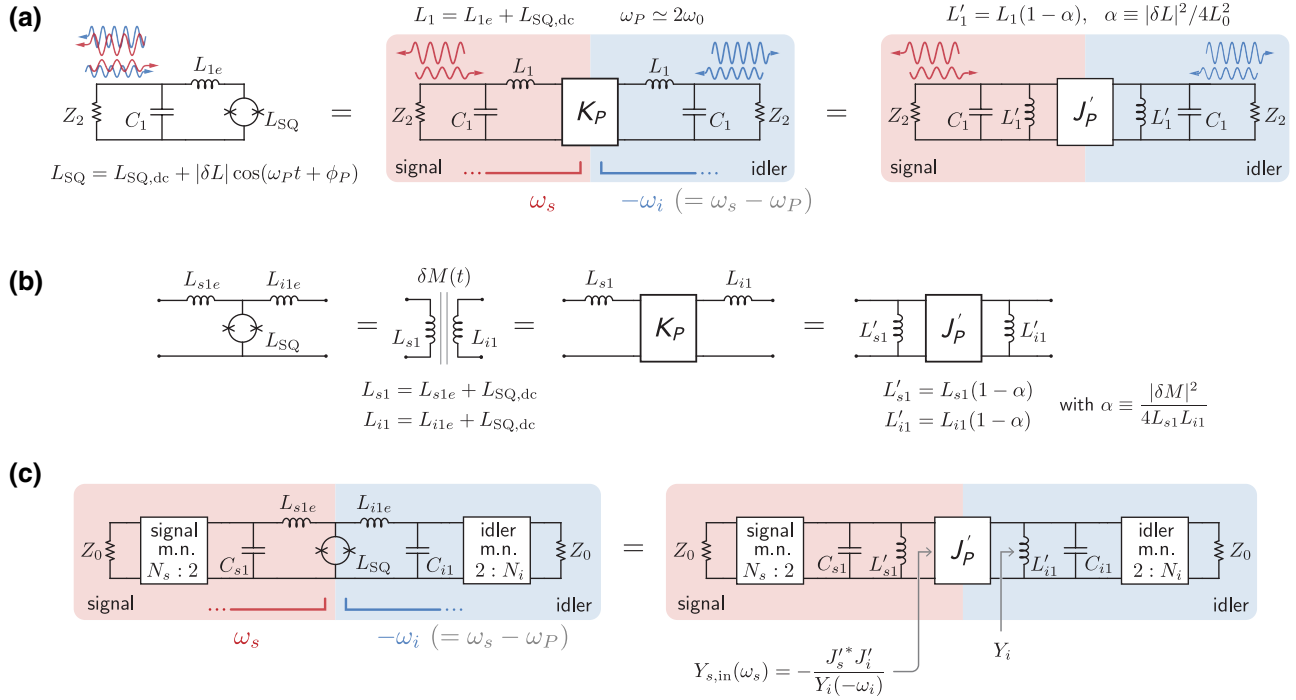
FIG. 24. (a) Transformation of single-pole degenerate Josephson parametric amplifier (left) to a two-port (signal and idler) series parametric inverter representation ($K_P$, middle), and a shunt parametric inverter representation ($J'_P$, right). (b) Equivalence between the parametrically modulated inductor tee and modulated mutual inductance circuits, and their $K$- and $J$-inverter counterparts. The inverter formulae are given in Fig. 9. (c) Example multipole matching strategy for a nondegenerate parametric amplifier using a parametric $J$ inverter. The tee-equivalent $J$ inverter transforms the SQUID-embedded double-resonator circuit into effective parallel-$LC$ sections of multipole signal and idler matching networks (m.n. in the figure). The input admittance looking into the inverter from the signal circuit $Y_{s,\text{in}}(\omega_s)$ is the nondegenerate equivalent to the pumpistor model admittance [49] since $Y_i^*(\omega_i) = Y_i(-\omega_i)$.

however, they are more general in that they allow one to obtain full two-port scattering parameters, since they treat the signal and idler ports equally. To be more concrete, in the degenerate parametric amplifier case, the incoming signal and idler tones are driven from the same *physical* port and then both re-emitted from the same *physical* port [see the left diagram in Fig. 24(a)]. This can still be described as a two-port scattering problem in the signal-idler basis, where the signal is the "left" *frequency* port and the idler is the "right" *frequency* port, as illustrated in the middle diagram of Fig. 24(a). Likewise, any matching network (e.g., Refs. [6,7]) would be mirrored on either side, but evaluated at the respective frequencies: $\omega_s$ on the signal side and $-\omega_i$ ($= \omega_s - \omega_P$) on the idler side. In a nondegenerate amplifier, the distinction between physical and frequency ports is not necessary, and the signal and idler matching networks can be physically distinct with different numbers of poles and filter types, allowing for more flexibility in design.

### 1. Degenerate parametric amplifier

In Figs. 8 and 9, we labeled the inverter equivalents as $K$ type or $J$ type, depending on the topology of the circuit in which they are embedded. When designing a

degenerate parametric amplifier around a flux- or current-pumped Josephson circuit, it is natural to resonate the Josephson circuit out using a parallel capacitor; see the left diagram of Fig. 24(a). In this case, since the parametrically modulated component is embedded in a parallel resonator, it is more convenient to use the "shunt representation" in Figs. 8 and 9, and model the parametric coupler as an admittance $J$ inverter; see the right diagram of Fig. 24(a). The full circuit can be analyzed by virtually mirroring it and evaluating each element at the signal and idler frequencies [Figs. 24(b) and 24(c)]. Note that we have included the possibility of stray inductance $L_{1e}$ in the transformation to a two-frequency-port circuit. We can then write out the total transmission ($ABCD$) matrix for this example by cascading the $ABCD$ matrices of the constituent components. For the single-pole amplifier in Fig. 24(a), we have

$$\mathbf{T}_\Sigma = \begin{bmatrix} 1 & 0 \\ j\omega_s C_1 & 1 \end{bmatrix} \begin{bmatrix} 1 & 0 \\ (j\omega_s L'_1)^{-1} & 1 \end{bmatrix} \begin{bmatrix} 0 & j/J'^*_s \\ -jJ'_i & 0 \end{bmatrix}$$

$$\times \begin{bmatrix} 1 & 0 \\ (-j\omega_i L'_1)^{-1} & 1 \end{bmatrix} \begin{bmatrix} 1 & 0 \\ -j\omega_i C_1 & 1 \end{bmatrix}, \quad \text{(C1)}$$

where the inverter constants $J_{s(i)}$ are defined in Fig. 8. From Eq. (C1), and assuming a port impedance $Z_2$ as in

Fig. 24(a), one can compute the scattering matrix [28], whose elements express the reflection (*cis-*)gains and conversion (*trans-*)gains versus frequency.

### 2. Nondegenerate amplifier

The single-pole design in the above section is simple, and can be easily extended to a nondegenerate amplifier. One starts with a modulated inductance with a value that is constrained by its physical realization (e.g., available critical current densities in a given process), and the center frequency of the amplifier can then be set by the value of $C_1$. The value of the terminating impedance $Z_2$ can be chosen to yield the desired bandwidth, $\Delta\omega = 1/2\pi Z_2 C_1$. In turn, $Z_2$ can be realized by transforming the 50 Ω source impedance using an immittance inverter (see Appendix D). In designs using multipole matching networks, the relative immittances of each of the sections can be systematically determined by the filter prototypes. In Sec. V D 1 we designed a coupled-mode network for a matched nondegenerate amplifier, but abstracted the physical details of the parametric coupler. Here we demonstrate a physical circuit synthesis procedure using the method of Sec. IV A and the parametric inverter model from Sec. III. Furthermore, whereas in Sec. V D 1 we assumed that the same prototype and bandwidth was used for both signal and idler ports, here we treat a more general synthesis problem that does not make this assumption.

We start with the circuit shown in the left diagram of Fig. 24(b) as the core of our design: an inductor tee where the center inductance is the modulated inductor (e.g., a Josephson circuit) and the arm inductances are required to form distinct tank circuits that make up the first resonator sections of arbitrary matching networks on the signal and idler sides. As we saw in Sec. IV A, filter sections are either parallel or series resonators yet the tee looks like neither. To begin our synthesis procedure, we transform the physical topology of this core element into an effective circuit comprised of two parallel-*LC* resonators, sandwiching a pure parametric *J*-type inverter. The steps for this transformation are summarized in Fig. 24(b). Indexing the filter sections from the core outwards, these resonators form the respective $k = 1$ sections of extended matching networks on the signal (labeled with subscript *s*) and idler (labeled with *i*) sides. Following Sec. IV A, we can relate the impedance of these sections to the reference impedances of the filter networks, $Z_{m,0}$:

$$Z_{m,1} = \omega_m L'_{m,1} = \frac{\omega_m}{\Delta\omega_m} \frac{Z_{m,0}}{g_{m,1}}. \tag{C2}$$

Here $g_{m,k}$ is the prototype coefficient corresponding to the *k*th section in the *m*th circuit, and with $m \in \{s, i\}$. Note that the reference impedances for the respective signal and idler circuits, $Z_{m,0}$, as extracted from Eq. (C2) *are not* generally going to be 50 Ω.

With the reference impedance found from Eq. (C2) and the prototype coefficients $\{g_{m,k}\}$, we can proceed to derive a circuit with alternating series and parallel resonators (Sec. IV A). As in the degenerate amplifier example above, the two-port scattering parameters can be calculated simply by computing the total transmission matrix product; however, in this case, the signal and idler modes correspond to separate physical circuits and ports.

Figure 25(a) shows a denormalized ladder circuit (alternating series and parallel resonators) computed for the three-pole (0.5-dB ripple) Chebyshev prototype we have already used in Sec. V D 1. Component values are indicated in the figure. Note that the terminating impedances of the signal port $Z_1$ and the idler port $Z_2$ are not 50 Ω; these can be transformed to 50 Ω by inserting admittance inverters as in, e.g., Sec. V D 2. Note also that the impedances of the series resonators in the circuit are rather high, producing inconvenient component values. These sections could be transformed to parallel resonators by use of additional inverters following Sec. IV B. The addition of physical admittance inverters, however, will invariably introduce additional frequency dependence in the circuit [57] that will become more pronounced in designs with either higher bandwidth, or greater frequency separation between the signal and the idler.



**(a)**

**(b)**
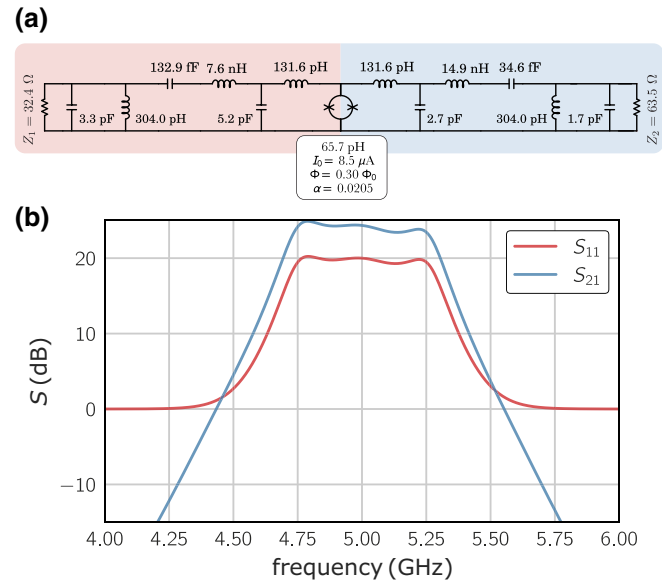
FIG. 25. (a) Example nondegenerate amplifier circuit based on the three-pole Chebyshev graph in Fig. 20, centered at 5 GHz (signal) and 7 GHz (idler). (b) Calculated *S* parameters for a matched parametric amplifier (referred to the port impedances $Z_1$ and $Z_2$, not to 50 Ω). Here $S_{11}$ is the signal reflection cisgain, and $S_{21}$ is the signal-idler trans-gain. In contrast to Fig. 20, these represent the power gain rather than the photon number gain; therefore, $S_{21}$ has an extra overall relative scaling factor $f_2 Z_2 / f_1 Z_1$ (4.4 dB at 5.0 GHz).

Figure 25(b) shows reflection and transmission gain for the circuit in panel (a), computed from its cascaded *ABCD* matrix. In contrast to Fig. 20(b), these represent the power gain rather than the photon number gain; therefore, $S_{21}$ has an extra overall relative scaling factor $f_2 Z_2 / f_1 Z_1$ (4.4 dB at 5.0 GHz). Also visible is a sloped gain profile, stemming from a frequency dependence of the parametric inverter itself; this effect is inherent to all physical implementations of nondegenerate parametric amplifiers [42], but is absent in calculations based on ideal (frequency-independent) coupling rates, such as in Fig. 20. Methods for equalizing the gain slope can be found in, e.g., Ref. [71]. Alternatively, one can slightly detune the $k = 1$ resonators [42].

### 3. Modulation amplitude $|\delta M|$

Here we show how to calculate the modulation amplitude in a general multipole parametric amplifier circuit. Knowledge of this parameter is useful for a few reasons. First, it gives the designer a basis for setting requirements on physical parameters such as the participation ratio of the modulated inductance to the total inductance, or the on-chip coupling strength of the ac bias line to the modulated component. Second, it helps determine whether the required inverter constant (in this example $J'_m$, as defined in Sec. III C and Figs. 8 and 9) is even physically tenable for a given Josephson circuit.

In Figs. 8 and 9, we parameterize the inverter constants and effective inductances in terms of a normalized modulation parameter $\alpha$. An expression for $\alpha$ can be derived by requiring that the parametric inverter, when looking from either its signal or idler side, transforms the opposite port's immittance to the correct value to yield the required reflection gain on resonance. For instance, looking into the $J'$ inverter from the signal side on resonance, as in the right diagram of Fig. 24(c), we see that an input admittance, Eq. (39), can be written as

$$
\begin{aligned}
Y_{s,\text{in}}(\omega = \omega_{s0}) &= -\frac{J'^*_s J'_i}{Y_{i,N_i+1}} \\
&= -\frac{\alpha}{\omega_{s0} L'_s \omega_{i0} L'_i Y_{i,N_i+1}}.
\end{aligned} \tag{C3}
$$

Here, $\omega_{s0}$ and $\omega_{i0}$ are the signal and idler center frequencies, $Y_{i,N_i+1}$ is the idler termination admittance, and we have used the definitions in Fig. 9(b). Note that only the terminating admittance $Y_{i,N_i+1}$ appears in Eq. (C3) because at the center frequency of the network all shunt resonators are effectively open circuit and all series resonators are short circuit, so that the network is effectively "transparent" and does not transform the value of the terminating admittance in any way. Setting $Y_{s,\text{in}}$ equal to the required value to obtain power gain $G$ in reflection, Sec. V D

($Y_{s,N_s+1}$ is the signal port termination admittance),

$$
Y_{s,\text{in}}(\omega = \omega_{s0}) = Y_{s,N_s+1} \frac{\sqrt{G} - 1}{\sqrt{G} + 1}, \tag{C4}
$$

we can, after recognizing the terms in the denominator of Eq. (C3) as denormalized filter section immittances, derive the following general form for the modulation amplitude:

$$
\begin{aligned}
\alpha &= \frac{|\delta M|^2}{4 L_{s,1} L_{i,1}} \\
&= \left[ \frac{\sqrt{G} + 1}{\sqrt{G} - 1} \right]^{\pm 1} \frac{\Delta \omega_s}{\omega_{s0}} \frac{\Delta \omega_i}{\omega_{i,0}} \frac{g_{s,N_s+1}^{p_s} g_{i,N_i+1}^{p_i}}{g_{s,1} g_{i,1}}.
\end{aligned} \tag{C5}
$$

The positive and negative signs in the exponent of the gain factor correspond to the use of series ($K$-type) and shunt ($J$-type) inverters, respectively. Likewise, Eq. (C5) is generalized to arbitrary filter orders for the signal and idler circuits, $N_{s(i)}$, different filter prototype coefficients, and differing fractional bandwidth specifications $\Delta \omega_m / \omega_{m0}$. The $p_{s(i)}$ are parity exponents that evaluate to $p_m = 1$ when $N_m$ is even, and $p_m = -1$ when $N_m$ is odd. This result expands on the examples we have given in the main text, where the same bandwidth and prototype was used for both signal and idler.

Since $\alpha$ is physically bounded by the $k = 1$ mode inductances, $\alpha \leq 1$, Eq. (C5) sets limits to the available bandwidth. Likewise, for a fixed bandwidth and gain, one finds that the normalized modulation amplitude $\sqrt{\alpha}$ gets smaller at increasing prototype order. In practical terms, this means that it gets easier to achieve the target gain as one increases the order of the matching network.

### APPENDIX D: INVERTERS AT TERMINATIONS

The canonical inverter realization consists of either a $\pi$ network (Fig. 11) or a tee network where the central element (a series or shunt reactance) is sandwiched between (shunt or series) elements with identical reactance values, except with the opposite sign [28,48]. When placed between two resonator circuits, these negative reactances can be absorbed into the reactances forming adjacent resonator sections. However, when an inverter is placed at a real termination, $Z_0$ (Fig. 26), there is no reactance at the termination to absorb the negative reactance. In this tutorial, we follow the standard practice and use an asymmetric two-element topology that places the negative reactance on one side [57]. One can equate the real and imaginary parts of the input admittance of the ideal inverted termination (Fig. 26, left) to the capacitive two-element topology (Fig. 26, right), and derive, for the series coupling
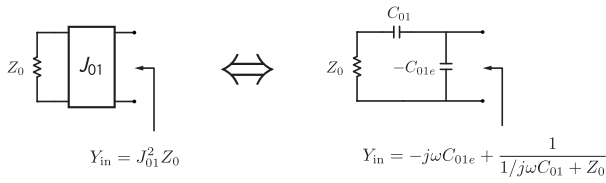
FIG. 26. Left: inverter at termination. Right: capacitive inverter equivalent.

capacitance,

$$C_{01} = \frac{J_{01}}{\omega_0} \frac{1}{\sqrt{1 - Z_0^2 J_{01}^2}}, \tag{D1}$$

shunted by a negative reactance $-C_{01e}$, where

$$C_{01e} = \frac{J_{01}}{\omega_0} \sqrt{1 - Z_0^2 J_{01}^2}. \tag{D2}$$

Here we have set $\omega = \omega_0$ so that this transformation is exact at the center frequency.

This particular topology is similar to the capacitive $\pi$ inverter, with a leg removed. The expressions are similar to the symmetric $\pi$ version, Fig. 11(b), but with a scaling factor that is dependent on the desired transformation ratio, since $Z_0^2 J_{01}^2 = Y_{in}/Y_0$ (with $Z_0 \equiv 1/Y_0$). One can derive a similar variant for the tee topology using the same approach. As in the canonical $\pi$ and tee topologies, this inverter is constructed with frequency-dependent reactances, so the inversion is only exactly correct at the center frequency $\omega_0$.

## APPENDIX E: CALCULATING PROTOTYPE COEFFICIENTS BY CAUER SYNTHESIS

Here, we briefly review the procedure for calculating prototype coefficients using the well-known *insertion loss* technique (cf. Ref. [28]) and Cauer synthesis [45]. The technique is based on the fact that the input impedance of a ladder circuit, as a function of frequency, can be expressed as a continued fraction, Eq. (E7). Since prototype tables for passively terminated filter networks are commonly available [28,57], we focus here on prototypes designed specifically for active, negative resistance loads, such as presented by parametric amplifiers.

We start with a power loss function, $P_L(\omega)$, which is an even function of frequency, normalized to a cutoff frequency of $2\pi \times 1$ Hz. This function is usually expressed as a polynomial of order $2N$, where $N$ usually corresponds to the number of reactances (for low-pass networks) or resonant modes (for band-pass networks) in the circuit. The

reflected power at the input of the network is given by

$$|\Gamma(\omega)|^2 = 1 - \frac{1}{P_L(\omega)} = \frac{P_L(\omega) - 1}{P_L(\omega)}. \tag{E1}$$

For Butterworth networks, $P_L$ can be written as

$$P_L(\omega) = A \left(1 + k^2 \omega^{2N}\right), \tag{E2}$$

and for Chebyshev networks, it can be written as

$$P_L(\omega) = A \left[1 + k^2 T_N^2(\omega)\right], \tag{E3}$$

where $T_N(\omega)$ is a Chebyshev polynomial of order $N$. In both expressions, $A \in [0, 1]$ controls the match ($P_L = 1$ means zero reflection), and $k^2$ controls the reflection at the cutoff frequency where $\omega = 1$.

### 1. Cauer synthesis

Our task is to factor Eq. (E1) into $|\Gamma(s)|^2 = \Gamma(s)\Gamma(-s)$, where $s = j\omega$. Note that we have a choice of sign for $\Gamma$: if we choose a positive sign then, when $\omega \to \infty$, the low-pass prototype looks like an open circuit, and we may use $\Gamma(s)$ to write the input impedance of the network (normalized to 1 $\Omega$) $Z(s) = [1 + \Gamma(s)]/[1 - \Gamma(s)]$. If we choose the negative sign then, when $\omega \to \infty$, the low-pass prototype looks like a short circuit, and we may use $\Gamma(s)$ instead to write the input admittance of the network (normalized to $1 \ \Omega^{-1}$) $Y(s) = [1 - \Gamma(s)]/[1 + \Gamma(s)]$.

Since $|\Gamma(s)|^2$ is a ratio of polynomials of order $2N$, $\Gamma(s)$ is a ratio of polynomials of order $N$, $\Gamma(s) = R(s)/D(s)$, where

$$R(s) = \prod_{i=1}^{N} (s - z_i), \tag{E4}$$

$$D(s) = \prod_{i=1}^{N} (s - p_i), \tag{E5}$$

where the $p_i$ are the complex roots of the denominator of $|\Gamma(s)|^2$ that are in the left half-plane (LHP), $\text{Re}\{p_i\} < 0$. The $z_i$ are the complex roots of the numerator of $|\Gamma(s)|^2$, which we pick either from the LHP or from the imaginary axis in conjugate pairs, or from the origin, until we have exactly $N$ of them.

We can then write (for a positive sign of $\Gamma$)

$$Z(s) = \frac{1 + \Gamma(s)}{1 - \Gamma(s)} = \frac{D(s) + R(s)}{D(s) - R(s)} \tag{E6}$$

or $Y(s) = 1/Z(s)$ (for a negative sign choice). Expanding out Eqs. (E4) and (E5) to polynomial form and substituting into Eq. (E6), we get a ratio of polynomials where the order of the numerator is greater than that of the denominator by 1.

From here, we proceed to use polynomial long division to write $Z(s)$, or $Y(s)$, as a continued fraction expansion (Cauer form):

$$Z = g_1 s + \cfrac{1}{g_2 s + \cfrac{1}{g_3 s + \cdots}}. \qquad (E7)$$

The coefficients $\{g_i\}$ of the Cauer expansion are the filter prototype coefficients. The procedure for writing the continued-fraction expansion for a fraction of polynomials and extracting $\{g_i\}$ can be automated using, e.g., the `numpy` PYTHON package, where the inputs `n` and `d` to the function below are the numerator and denominator polynomials of the impedance (or the admittance), Eq. (E6), respectively.

```
import numpy as np
def cauer(n: np.poly1d, d: np.poly1d):
    assert n.order == d.order + 1
    g = [1.0]
    while n.order > 0:
        quot, rem = np.polydiv(n, d)
        g.append(quot.coef[0])
        n = d
        d = rem
    g.append(1 / quot.coef[-1])
    return g
```

### 2. Prototype synthesis for negative resistance amplifiers

In Sec. V D we saw that the reflection gain from an active negative-resistance load is equivalent to the return loss from a passive termination having the same absolute value of resistance. However, gain in the signal mode also necessitates gain in the idler mode, and because the amplified signals are correlated [72], the power loss function that we need to use when synthesizing a matching network should be calculated based on the gain parameter:

$$G_{\mathrm{PL}} = \left(\sqrt{G} + \sqrt{G-1}\right)^2 = 4G - 2 + \mathcal{O}\!\left(\frac{1}{G}\right) \quad (E8)$$

with $G$ the *signal* power gain. This is in contrast to Ref. [47], which assumes that the amplified signal and idler are not correlated.

In other words, if $P_s$ is the input signal power then $G_{\mathrm{PL}} P_s$ is the power extracted from the pump. The matching network must be designed to allow this power to be dissipated in both the signal and idler terminations.

#### a. Butterworth response

For the Butterworth response type, we set $A$ in Eq. (E2) so that $|\Gamma(0)|^2 = 1/G_{\mathrm{PL}}$, and $k^2$ in Eq. (E2) so that at the

TABLE II. Butterworth coefficients calculated according to Appendix E for several amplifier gains, and for two-, three-, and four-section networks, using the power loss function in Eq. (E9). Coefficient $g_0$ refers to the active load.

| Signal gain $G$ (dB) | Order | $g_0$ | $g_1$ | $g_2$ | $g_3$ | $g_4$ | $g_5$ |
|---|---|---|---|---|---|---|---|
| 15 | 2 | 1.0 | 0.6067 | 0.2733 | 1.1969 | | |
|    | 3 | 1.0 | 0.8122 | 0.6587 | 0.3710 | 0.8355 | |
|    | 4 | 1.0 | 0.9266 | 0.8729 | 0.9049 | 0.2266 | 1.1969 |
| 17 | 2 | 1.0 | 0.5149 | 0.2587 | 1.1528 | | |
|    | 3 | 1.0 | 0.7078 | 0.6417 | 0.3381 | 0.8674 | |
|    | 4 | 1.0 | 0.8175 | 0.8613 | 0.8361 | 0.2263 | 1.1528 |
| 20 | 2 | 1.0 | 0.4085 | 0.2343 | 1.1055 | | |
|    | 3 | 1.0 | 0.5846 | 0.6073 | 0.2981 | 0.9045 | |
|    | 4 | 1.0 | 0.6878 | 0.8309 | 0.7527 | 0.2225 | 1.1055 |
| 25 | 2 | 1.0 | 0.2852 | 0.1921 | 1.0579 | | |
|    | 3 | 1.0 | 0.4372 | 0.5371 | 0.2468 | 0.9453 | |
|    | 4 | 1.0 | 0.5310 | 0.7594 | 0.6461 | 0.2103 | 1.0579 |
| 30 | 2 | 1.0 | 0.2035 | 0.1531 | 1.0321 | | |
|    | 3 | 1.0 | 0.3352 | 0.4631 | 0.2071 | 0.9689 | |
|    | 4 | 1.0 | 0.4206 | 0.6775 | 0.5630 | 0.1941 | 1.0321 |

cutoff frequency $|\Gamma(1)|^2 = 2/G_{\mathrm{PL}}$, to define the amplifier bandwidth as the half-gain points (3-dB bandwidth).

The power loss function we use to generate normalized Butterworth low-pass prototypes of order $N$ for a desired signal power gain $G$ is therefore given by

$$P_L(\omega) = \frac{G_{\mathrm{PL}}}{G_{\mathrm{PL}} - 1}\left[1 + \left(\frac{1}{G_{\mathrm{PL}} - 2}\right)\omega^{2N}\right], \qquad (E9)$$

where $G_{\mathrm{PL}}$ is defined in Eq. (E8). Calculated prototype coefficients for a practical selection of gains are listed in Table II.

#### b. Chebyshev response

For the Chebyshev response type, for a given order $N$, and specified signal gain $G_0$ in dB, and gain ripple $R$ in dB, we define

$$G_{\mathrm{min}}^{\mathrm{dB}} = \begin{cases} G_0, & N \text{ even}, \\ G_0 - R, & N \text{ odd}, \end{cases} \qquad (E10)$$

and

$$G_{\mathrm{max}}^{\mathrm{dB}} = \begin{cases} G_0 + R, & N \text{ even}, \\ G_0, & N \text{ odd}. \end{cases} \qquad (E11)$$

If $G_{\mathrm{max}}$ and $G_{\mathrm{min}}$ are the corresponding signal power gains in *linear* power units then we should calculate the power loss function in terms of $G_{\mathrm{max}}^{\mathrm{PL}} = 4G_{\mathrm{max}} - 2$ and

TABLE III.   Chebyshev coefficients calculated according to Appendix E for several values of amplifier gain and gain ripple, and for two-, three-, and four-section networks, using the power loss function in Eq. (E12). Coefficient $g_0$ refers to the active load.

| Signal gain $G$ (dB) | Ripple $R$ (dB) | Order | $g_0$ | $g_1$ | $g_2$ | $g_3$ | $g_4$ | $g_5$ |
|---|---|---|---|---|---|---|---|---|
| 17 | 0.1 | 2 | 1.0 | 0.2769 | 0.1451 | 1.1528 | | |
| | | 3 | 1.0 | 0.5595 | 0.5410 | 0.3098 | 0.8674 | |
| | | 4 | 1.0 | 0.7489 | 0.8450 | 0.9181 | 0.2767 | 1.1528 |
| | 0.5 | 2 | 1.0 | 0.3981 | 0.2206 | 1.1528 | | |
| | | 3 | 1.0 | 0.7062 | 0.7029 | 0.4326 | 0.8674 | |
| | | 4 | 1.0 | 0.8533 | 0.9943 | 1.1289 | 0.3667 | 1.1528 |
| | 1.0 | 2 | 1.0 | 0.4567 | 0.2642 | 1.1527 | | |
| | | 3 | 1.0 | 0.7822 | 0.7854 | 0.5095 | 0.8674 | |
| | | 4 | 1.0 | 0.8892 | 1.0592 | 1.2252 | 0.4182 | 1.1527 |
| 20 | 0.1 | 2 | 1.0 | 0.2204 | 0.1310 | 1.1055 | | |
| | | 3 | 1.0 | 0.4656 | 0.5126 | 0.2707 | 0.9045 | |
| | | 4 | 1.0 | 0.6370 | 0.8200 | 0.8243 | 0.2683 | 1.1055 |
| | 0.5 | 2 | 1.0 | 0.3184 | 0.1982 | 1.1055 | | |
| | | 3 | 1.0 | 0.5899 | 0.6681 | 0.3753 | 0.9045 | |
| | | 4 | 1.0 | 0.7296 | 0.9671 | 1.0147 | 0.3525 | 1.1055 |
| | 1.0 | 2 | 1.0 | 0.3666 | 0.2366 | 1.1055 | | |
| | | 3 | 1.0 | 0.6545 | 0.7488 | 0.4397 | 0.9045 | |
| | | 4 | 1.0 | 0.7629 | 1.0310 | 1.1032 | 0.3999 | 1.1055 |
| 25 | 0.1 | 2 | 1.0 | 0.1546 | 0.1069 | 1.0579 | | |
| | | 3 | 1.0 | 0.3520 | 0.4541 | 0.2214 | 0.9453 | |
| | | 4 | 1.0 | 0.4997 | 0.7559 | 0.7044 | 0.2485 | 1.0579 |
| | 0.5 | 2 | 1.0 | 0.2246 | 0.1608 | 1.0579 | | |
| | | 3 | 1.0 | 0.4487 | 0.5939 | 0.3039 | 0.9453 | |
| | | 4 | 1.0 | 0.5768 | 0.8950 | 0.8679 | 0.3226 | 1.0579 |
| | 1.0 | 2 | 1.0 | 0.2599 | 0.1912 | 1.0579 | | |
| | | 3 | 1.0 | 0.4992 | 0.6682 | 0.3537 | 0.9453 | |
| | | 4 | 1.0 | 0.6060 | 0.9554 | 0.9450 | 0.3632 | 1.0579 |
| 30 | 0.1 | 2 | 1.0 | 0.1107 | 0.0849 | 1.0321 | | |
| | | 3 | 1.0 | 0.2722 | 0.3920 | 0.1839 | 0.9689 | |
| | | 4 | 1.0 | 0.4013 | 0.6794 | 0.6112 | 0.2256 | 1.0321 |
| | 0.5 | 2 | 1.0 | 0.1615 | 0.1272 | 1.0321 | | |
| | | 3 | 1.0 | 0.3488 | 0.5139 | 0.2506 | 0.9689 | |
| | | 4 | 1.0 | 0.4663 | 0.8071 | 0.7530 | 0.2899 | 1.0321 |
| | 1.0 | 2 | 1.0 | 0.1875 | 0.1507 | 1.0321 | | |
| | | 3 | 1.0 | 0.3892 | 0.5796 | 0.2901 | 0.9689 | |
| | | 4 | 1.0 | 0.4918 | 0.8630 | 0.8204 | 0.3245 | 1.0321 |

$G_{\min}^{\mathrm{PL}} = 4G_{\min} - 2$, similar to Eq. (E8). The power loss function can then be written as

$$P_L(\omega) = \frac{G_{\max}^{\mathrm{PL}}}{G_{\max}^{\mathrm{PL}} - 1}\left[1 + \left(\frac{1}{G_{\min}^{\mathrm{PL}}} - \frac{1}{G_{\max}^{\mathrm{PL}}}\right)T_N^2(\omega)\right].$$

(E12)

Note that, for the Chebyshev response, the parameter $k^2$ in Eq. (E3) does not correspond to the 3-dB (half-gain) points, but rather, it controls the bandwidth over which the gain oscillates by the ripple amount [28]. Therefore, the 3-dB bandwidth of the amplifier will generally be greater than the specified bandwidth parameter $\Delta\omega$ that

appears in Secs. IV and V. Calculated prototype coefficients for a practical selection of gain and ripple specifications are listed in Table III. Additional listings are given in Refs. [47,57]; however, the gain specified therein is the total gain in both signal and idler bands, leading roughly to a 6 dB difference from our definition: what we denote as $G = 20$ dB would appear as $G \approx 26$ dB in the convention of Refs. [47,57].

## APPENDIX F: CAUER FORM OF A 1D ARRAY OF NEAREST-NEIGHBOR COUPLED MODES USING GRAPH REDUCTION

We start by looking at the example of Fig. 7 for a four-mode circuit and then generalize. Equation (27) writes the

reduced-mode detuning term for the system as

$$\Delta_1' = \Delta_1 - \cfrac{\beta_{12}^2}{\Delta_2 - \cfrac{\beta_{23}^2}{\Delta_3 - \cfrac{\beta_{34}^2}{\Delta_4}}}. \tag{F1}$$

For a 1D simply connected system, we can take $\beta_{jk}$ to be real, so we drop the absolute value in $|\beta_{jk}|^2$ compared to Eq. (27).

We make the resonant pump assumption, and change the variable to a normalized detuning, as common in microwave engineering:

$$s = -2i\frac{\omega - \omega_0}{\Delta\omega}. \tag{F2}$$

Here $\omega$ is the signal frequency, $\omega_0$ is the mode frequency, and $\Delta\omega$ is the bandwidth. With this substitution we can write the detuning terms appearing in Eq. (F1) as

$$\Delta_1 = i\frac{\Delta\omega}{2\gamma_0}s + i\frac{\gamma_{01}}{2\gamma_0}, \tag{F3}$$

$$\Delta_2 = \Delta_3 = i\frac{\Delta\omega}{2\gamma_0}s, \tag{F4}$$

$$\Delta_4 = i\frac{\Delta\omega}{2\gamma_0}s + i\frac{\gamma_{45}}{2\gamma_0}. \tag{F5}$$

Substituting this into Eq. (F1) and using Eq. (26), we can write the admittance seen from the port (after some algebra) as

$$\frac{Y}{Y_0} = 2\left(\frac{\beta_{12}\beta_{34}}{\beta_{23}}\right)^2\frac{\gamma_0}{\gamma_{01}}\left[g_1 s + \cfrac{1}{g_2 s + \cfrac{1}{g_3 s + \cfrac{1}{g_4 s + \cfrac{1}{g_5}}}}\right], \tag{F6}$$

where we have defined

$$g_1 = \left(\frac{\beta_{23}}{\beta_{12}\beta_{34}}\right)^2\frac{\Delta\omega}{2\gamma_0},$$

$$g_2 = \left(\frac{\beta_{34}}{\beta_{23}}\right)^2\frac{\Delta\omega}{2\gamma_0},$$

$$g_3 = \left(\frac{1}{\beta_{34}}\right)^2\frac{\Delta\omega}{2\gamma_0},$$

$$g_4 = \frac{\Delta\omega}{2\gamma_0},$$

$$g_5 = \frac{2\gamma_0}{\gamma_{45}}.$$

We further define $g_0$ as the prefactor in Eq. (F6). This brings the continued-fraction expression for the admittance, Eq. (F6), to exact equivalence with the Cauer expansion in Appendix E. The coefficients $\{g_i\}$ are the prototype coefficients of the normalized low-pass network (cf. Sec. IV) that represents the circuit.

Looking at products of the form $g_j g_{j+1}$, and generalizing to a 1D coupled system of $N$ modes, we obtain

$$g_0 g_1 = \frac{\Delta\omega}{\gamma_{01}},$$

$$g_j g_{j+1} = \frac{1}{\beta_{j,j+1}^2}\left(\frac{\Delta\omega}{2\gamma_0}\right)^2,$$

$$g_N g_{N+1} = \frac{\Delta\omega}{\gamma_{N,N+1}},$$

which are equivalent to Eqs. (60)–(62).

———————

[1] J. Aumentado, Superconducting parametric amplifiers: The state of the art in Josephson parametric amplifiers, IEEE Microw. Mag. **21**, 45 (2020).

[2] R. Vijay, D. Slichter, and I. Siddiqi, Observation of Quantum Jumps in a Superconducting Artificial Atom, Phys. Rev. Lett. **106**, 110502 (2011).

[3] L. Ranzani and J. Aumentado, Circulators at the quantum limit: Recent realizations of quantum-limited superconducting circulators and related approaches, IEEE Microw. Mag. **20**, 112 (2019).

[4] C. Macklin, K. O'Brien, D. Hover, M. Schwartz, V. Bolkhovsky, X. Zhang, W. Oliver, and I. Siddiqi, A near–quantum-limited Josephson traveling-wave parametric amplifier, Science **350**, 307 (2015).

[5] J. Y. Mutus, T. C. White, R. Barends, Y. Chen, Z. Chen, B. Chiaro, A. Dunsworth, E. Jeffrey, J. Kelly, and A. Megrant *et al.*, Strong environmental coupling in a Josephson parametric amplifier, Appl. Phys. Lett. **104**, 263513 (2014).

[6] T. Roy, S. Kundu, M. Chand, A. M. Vadiraj, A. Ranadive, N. Nehra, M. P. Patankar, J. Aumentado, A. A. Clerk, and R. Vijay, Broadband parametric amplification with impedance engineering: Beyond the gain-bandwidth product, Appl. Phys. Lett. **107**, 262601 (2015).

[7] O. Naaman, D. Ferguson, A. Marakov, M. Khalil, W. Koehl, and R. Epstein, in *2019 IEEE MTT-S International Microwave Symposium (IMS)* (IEEE, 2019), p. 259.

[8] N. E. Frattini, V. V. Sivak, A. Lingenfelter, S. Shankar, and M. H. Devoret, Optimizing the Nonlinearity and Dissipation of a SNAIL Parametric Amplifier for Dynamic Range, Phys. Rev. Appl. **10**, 054020 (2018).

[9] F. Lecocq, L. Ranzani, G. Peterson, K. Cicak, R. Simmonds, J. Teufel, and J. Aumentado, Nonreciprocal Microwave Signal Processing with a Field-Programmable Josephson Amplifier, Phys. Rev. Appl. **7**, 024028 (2017).

[10] K. Sliwa, M. Hatridge, A. Narla, S. Shankar, L. Frunzio, R. Schoelkopf, and M. Devoret, Reconfigurable Josephson Circulator/directional Amplifier, Phys. Rev. X **5**, 041020 (2015).

[11] B. Abdo, N. T. Bronn, O. Jinka, S. Olivadese, A. D. Córcoles, V. P. Adiga, M. Brink, R. E. Lake, X. Wu, and D. P. Pappas *et al.*, Active protection of a superconducting qubit with an interferometric Josephson isolator, Nat. Commun. **10**, 1 (2019).

[12] F. Lecocq, L. Ranzani, G. Peterson, K. Cicak, X. Jin, R. Simmonds, J. Teufel, and J. Aumentado, Efficient Qubit Measurement with a Nonreciprocal Microwave Amplifier, Phys. Rev. Lett. **126**, 020502 (2021).

[13] G. A. Peterson, F. Lecocq, K. Cicak, R. W. Simmonds, J. Aumentado, and J. D. Teufel, Demonstration of Efficient Nonreciprocity in a Microwave Optomechanical Circuit, Phys. Rev. X **7**, 031001 (2017).

[14] B. J. Chapman, E. I. Rosenthal, J. Kerckhoff, B. A. Moores, L. R. Vale, J. Mates, G. C. Hilton, K. Lalumiere, A. Blais, and K. Lehnert, Widely Tunable On-Chip Microwave Circulator for Superconducting Quantum Circuits, Phys. Rev. X **7**, 041043 (2017).

[15] R. W. Andrews, R. W. Peterson, T. P. Purdy, K. Cicak, R. W. Simmonds, C. A. Regal, and K. W. Lehnert, Bidirectional and efficient conversion between microwave and optical light, Nat. Phys. **10**, 321 (2014).

[16] M. Mirhosseini, A. Sipahigil, M. Kalaee, and O. Painter, Superconducting qubit to optical photon transduction, Nature **588**, 599 (2020).

[17] X. Han, W. Fu, C. Zhong, C.-L. Zou, Y. Xu, A. Al Sayem, M. Xu, S. Wang, R. Cheng, and L. Jiang *et al.*, Cavity piezo-mechanics for superconducting-nanophotonic quantum interface, Nat. Commun. **11**, 1 (2020).

[18] L. Ranzani and J. Aumentado, Graph-based analysis of nonreciprocity in coupled-mode systems, New J. Phys. **17**, 023024 (2015).

[19] G. A. Peterson, Ph.D. thesis, University of Colorado at Boulder, 2020.

[20] F. Lecocq, L. Ranzani, G. Peterson, K. Cicak, A. Metelmann, S. Kotler, R. Simmonds, J. Teufel, and J. Aumentado, Microwave Measurement beyond the Quantum Limit with a Nonreciprocal Amplifier, Phys. Rev. Appl. **13**, 044005 (2020).

[21] U. Vool and M. Devoret, Introduction to quantum electromagnetic circuits, Int. J. Circuit Theory and Appl. **45**, 897 (2017).

[22] Y. Y. Gao, M. A. Rol, S. Touzard, and C. Wang, A practical guide for building superconducting quantum devices, arXiv preprint arXiv:2106.06173 (2021).

[23] D. G. Tucker, *Circuits with Periodically-Varying Parameters: Including Modulators and Parametric Amplifiers* (van Nostrand Company, Inc., Princeton, NJ, 1964).

[24] H. J. Kimble, Strong interactions of single atoms and photons in cavity QED, Phys. Scr. **T76**, 127 (1998).

[25] A. Clerk, K. Lehnert, P. Bertet, J. Petta, and Y. Nakamura, Hybrid quantum systems with circuit quantum electrodynamics, Nat. Phys. **16**, 257 (2020).

[26] M. Aspelmeyer, T. J. Kippenberg, and F. Marquardt, Cavity optomechanics, Rev. Mod. Phys. **86**, 1391 (2014).

[27] B. Yurke, in *Quantum Squeezing* (Springer, 2004), p. 53.

[28] D. M. Pozar, *Microwave Engineering* (John Wiley & Sons, Hoboken, NJ, 2009).

[29] J. M. Manley and H. E. Rowe, Some general properties of nonlinear elements-part i. general energy relations, Proc. IRE **44**, 904 (1956).

[30] S. B. Cohn, Dissipation loss in multiple-coupled-resonator filters, Proc. IRE **47**, 1342 (1959).

[31] M. Dishal, Design of dissipative band-pass filters producing desired exact amplitude-frequency characteristics, Proc. IRE **37**, 1050 (1949).

[32] I. Hunter, A. Guyette, and R. Pollard, Passive microwave receive filter networks using low-Q resonators, IEEE Microw. Mag. **6**, 46 (2005).

[33] G. Andersson, S. W. Jolin, M. Scigliuzzo, R. Borgani, M. O. Tholén, D. B. Haviland, and P. Delsing, Squeezing and correlations of multiple modes in a parametric acoustic cavity, arXiv preprint arXiv:2007.05826 (2020).

[34] F. Lecocq, J. B. Clark, R. W. Simmonds, J. Aumentado, and J. D. Teufel, Quantum Nondemolition Measurement of a Nonclassical State of a Massive Object, Phys. Rev. X **5**, 041037 (2015).

[35] R. A. Brualdi and H. J. Ryser *et al.*, *Combinatorial Matrix Theory* (Taylor & Francis Group, Boca Raton, FL, 1991), 39.

[36] J. Greenman, Graphs and determinants, The Mathematical Gazette **60**, 241 (1976).

[37] B. Yurke, L. R. Corruccini, P. G. Kaminsky, L. W. Rupp, A. D. Smith, A. H. Silver, R. W. Simon, and E. A. Whittaker, Observation of parametric amplification and deamplification in a Josephson parametric amplifier, Phys. Rev. A **39**, 2519 (1989).

[38] J. Mutus, T. White, E. Jeffrey, D. Sank, R. Barends, J. Bochmann, Y. Chen, Z. Chen, B. Chiaro, and A. Dunsworth *et al.*, Design and characterization of a lumped element single-ended superconducting microwave parametric amplifier with on-chip flux bias line, Appl. Phys. Lett. **103**, 122602 (2013).

[39] B. Abdo, A. Kamal, and M. Devoret, Nondegenerate three-wave mixing with the Josephson ring modulator, Phys. Rev. B **87**, 014508 (2013).

[40] W. H. Louisell, *Coupled Mode and Parametric Electronics* (John Wiley & Sons, Inc., New York City, NY, 1960).

[41] L. A. Blackwell and K. L. Kotzebue, *Semiconductor-Diode Parametric Amplifiers* (Prentice-Hall, Inc., Englewood Cliffs, NJ, 1961).

[42] G. L. Matthaei, A study of the optimum design of wide-band parametric amplifiers and up-converters, IRE Trans. MTT **9**, 23 (1961).

[43] B. T. Henoch, A new method for designing wide-band parametric amplifiers, IEEE Trans. Microw. Theory Tech. **11**, 62 (1963).

[44] F. Dorfler and F. Bullo, Kron reduction of graphs with applications to electrical networks, IEEE Trans. Circuits Syst. I: Regular Papers **60**, 150 (2012).

[45] V. Aatre, *Network Theory and Filter Design* (New Age International Ltd., New Delhi, 1986).

[46] D. J. Parker, M. Savytskyi, W. Vine, A. Laucht, T. Duty, A. Morello, A. L. Grimsmo, and J. J. Pla, A near-ideal degenerate parametric amplifier, arXiv preprint arXiv:2108.10471 (2021).

[47] W. J. Getsinger, Prototypes for use in broadbanding reflection amplifiers, IEEE Trans. MTT **11**, 486 (1963).

[48] R. E. Collin, *Foundations for Microwave Engineering* (John Wiley & Sons, New Delhi, 2007).

[49] K. M. Sundqvist and P. Delsing, Negative-resistance models for parametrically flux-pumped superconducting quantum interference devices, EPJ Quantum Technol. **1**, 1 (2014).

[50] M. S. Allman, F. Altomare, J. D. Whittaker, K. Cicak, D. Li, A. Sirois, J. Strong, J. D. Teufel, and R. W. Simmonds, rf-SQUID-Mediated Coherent Tunable Coupling between a Superconducting Phase Qubit and a Lumped-Element Resonator, Phys. Rev. Lett. **104**, 177004 (2010).

[51] Y. Chen *et al.*, Qubit Architecture with High Coherence and Fast Tunable Coupling, Phys. Rev. Lett. **113**, 220502 (2014).

[52] O. Naaman, M. O. Abutaleb, C. Kirby, and M. Rennie, On-chip Josephson junction microwave switch, Appl. Phys. Lett. **108**, 112601 (2016).

[53] F. Yan, P. Krantz, Y. Sung, M. Kjaergaard, D. L. Campbell, T. P. Orlando, S. Gustavsson, and W. D. Oliver, Tunable Coupling Scheme for Implementing High-Fidelity Two-Qubit Gates, Phys. Rev. Appl. **10**, 054062 (2018).

[54] R. J. Cameron, Advanced coupling matrix synthesis techniques for microwave filters, IEEE Trans. Microw. Theory Tech. **51**, 1 (2003).

[55] H.-C. Liu and A. Yariv, Synthesis of high-order bandpass filters based on coupled-resonator optical waveguides (CROWs), Opt. Express **19**, 17653 (2011).

[56] R. J. Cameron, C. M. Kudsia, and R. R. Mansour, *Microwave Filters for Communication Systems: Fundamentals, Design, and Applications* (John Wiley & Sons, Inc., Hoboken, NJ, 2018).

[57] G. Matthaei, L. Young, and E. Jones, Microwave filters, impedance-matching networks, and coupling structures (artech microwave library), Artech House, February (Artech House, Norwood, MA, 1980).

[58] J. Rhodes, Modern filter theory and design, edited by gc temes and sk mitra, wiley, new york, 1973 (1975).

[59] L. Kinsler, A. Frey, A. Coppens, and J. Sanders, *Fundamentals of Acoustics* (John Wiley & Sons, Inc., New York City, NY, 2000).

[60] C. Madsen and J. Zhao, *Optical Filter Design and Analysis: A Signal Processing Approach*, Wiley Series in Microwave and Optical Engineering (John Wiley & Sons, Inc., New York City, NY, 1999).

[61] C.-H. Wang, M. Zhang, and L. Jiang, Generalized matching condition for unity efficiency quantum transduction, arXiv preprint arXiv:2202.06960 (2022).

[62] C.-H. Wang, F. Li, and L. Jiang, Quantum capacities of transducers, arXiv preprint arXiv:2203.00012 (2022).

[63] WRspice circuit simulator, http://www.wrcad.com/wrspice.html.

[64] L. K. Anderson, An analysis of broadband circulators with external tuning elements, IEEE Trans. MTT **15**, 42 (1967).

[65] J. Grebel, A. Bienfait, É. Dumur, H.-S. Chang, M.-H. Chou, C. R. Conner, G. A. Peairs, R. G. Povey, Y. P. Zhong, and A. N. Cleland, Flux-pumped impedance-engineered broadband Josephson parametric amplifier, Appl. Phys. Lett. **118**, 142601 (2021).

[66] P. Duan, Z. Jia, C. Zhang, L. Du, H. Tao, X. Yang, L. Guo, Y. Chen, H. Zhang, Z. Peng, W. Kong, H.-O. Li, G. Cao, and G.-P. Guo, Broadband flux-pumped Josephson parametric amplifier with an on-chip coplanar waveguide impedance transformer, Appl. Phys. Express **14**, 042011 (2021).

[67] O. Naaman, J. A. Strong, D. G. Ferguson, J. Egan, N. Bailey, and R. T. Hinkey, Josephson junction microwave modulators for qubit control, J. Appl. Phys. **121**, 073904 (2017).

[68] G. Liu, V. Josh, A. Lingenfelter, N. Frattini, S. Shankar, and M. Devoret, Minimal construction of fully directional parametric amplifier, Bulletin of the American Physical Society (2021).

[69] B. D. Josephson, Possible new effects in superconductive tunnelling, Phys. Lett. **1**, 251 (1962).

[70] J. Clarke and A. I. Braginski, *The SQUID Handbook: Applications of SQUIDs and SQUID Systems* (Wiley-VCH Verlag GmbH & Co. KGaA, Weinheim, 2006).

[71] D. Mellor and J. Linvill, Synthesis of interstage networks of prescribed gain versus frequency slopes, IEEE Trans. Microw. Theory Tech. **23**, 1013 (1975).

[72] M. Hatridge, R. Vijay, D. Slichter, J. Clarke, and I. Siddiqi, Dispersive magnetometry with a quantum limited SQUID parametric amplifier, Phys. Rev. B **83**, 134501 (2011).